SUPPORTING INFORMATION

Steric and Electronic Influence of Aryl Isocyanides on the Properties of Iridium(III) Cyclometalates

Ayan Maity, Linh Q. Le, Zhuan Zhu, Jiming Bao, and Thomas S. Teets

Contents

Index	*Page*
X-ray crystallographic data of **1a, 2a, 3b, 3c** and **4a**	2
UV-vis absorption and emission spectra of compounds **1a–4c**	4
Overlaid cyclic voltammograms of compounds **1a–4c**	10
NMR spectra for all new compounds	12

Table S1. Crystallographic data for **1a**, **2a**, and **3b**.

	1a·CH_2Cl_2	**2a**·$CHCl_3$	**3b**·$2CHCl_3$
Crystal data			
Chemical formula	$C_{42}H_{36}Cl_2F_3IrN_4O_3S$	$C_{41}H_{31}Cl_3F_{10}IrN_4P$	$C_{54}H_{52}Cl_6F_6IrN_4PS_2$
M_r	996.91	1099.22	1370.98
Crystal system, space group	Monoclinic, $P2_1/c$	Triclinic, $P\overline{1}$	Monoclinic, Pc
a, b, c (Å)	13.062 (3), 15.725 (4), 20.565 (5)	9.4166 (13), 10.9988 (15), 21.153 (3)	13.131 (2), 18.910 (3), 12.882 (2)
α, β, γ (°)	90, 106.358 (4), 90	98.7754 (17), 101.9794 (17), 103.7345 (18)	90, 117.880 (2), 90
V (Å^3)	4053.0 (18)	2034.4 (5)	2827.3 (9)
Z	4	2	2
μ (mm^{-1})	3.54	3.60	2.81
Crystal size (mm)	0.40 × 0.30 × 0.25	0.50 × 0.40 × 0.40	0.30 × 0.10 × 0.02
Data collection			
T_{min}, T_{max}	0.601, 0.746	0.584, 0.746	0.551, 0.746
No. of measured, independent and observed [$I > 2\sigma(I)$] reflections	26244, 10311, 8794	13390, 9793, 9443	16315, 9344, 8063
R_{int}	0.025	0.012	0.040
$(\sin \theta/\lambda)_{max}$ (Å^{-1})	0.691	0.689	0.692
Refinement			
$R[F^2 > 2\sigma(F^2)]$, $wR(F^2)$, S	0.031, 0.082, 1.04	0.026, 0.066, 1.11	0.034, 0.068, 0.91
No. of reflections	10311	9793	9344
No. of parameters	528	545	675
No. of restraints	121	0	2
	$w = 1/[\sigma^2(F_o^2) + (0.042P)^2 + 5.6072P]$ where $P = (F_o^2 + 2F_c^2)/3$	$w = 1/[\sigma^2(F_o^2) + (0.0282P)^2 + 4.4644P]$ where $P = (F_o^2 + 2F_c^2)/3$	$w = 1/[\sigma^2(F_o^2)]$ where $P = (F_o^2 + 2F_c^2)/3$
$\Delta\rho_{max}$, $\Delta\rho_{min}$ (e Å^{-3})	2.11, -1.12	2.21, -1.39	1.67, -1.71
Absolute structure	–	–	Classical Flack method preferred over Parsons because s.u. lower.
Absolute structure parameter	–	–	0.000 (5)

Table S2. Crystallographic data for **3c** and **4a**.

	3c·3CHCl$_3$	**4a**
Crystal data		
Chemical formula	$C_{51}H_{33}Cl_9F_6IrN_4PS_2$	$C_{44}H_{34}F_6IrN_4PS_2$
M_r	1422.15	1020.04
Crystal system, space group	Monoclinic, $P2_1/n$	Trigonal, $P3_221$
a, b, c (Å)	16.006 (2), 12.8079 (17), 27.606 (4)	16.325 (5), 16.325 (5), 26.077 (9)
α, β, γ (°)	90, 92.3505 (17), 90	90, 90, 120
V (Å^3)	5654.7 (13)	6019 (4)
Z	4	6
μ (mm^{-1})	2.95	3.54
Crystal size (mm)	0.40 × 0.30 × 0.20	0.15 × 0.10 × 0.10
Data collection		
T_{min}, T_{max}	0.612, 0.746	0.651, 0.746
No. of measured, independent and observed [$I > 2\sigma(I)$] reflections	36286, 14320, 11972	39006, 10196, 9865
R_{int}	0.023	0.030
$(\sin \theta/\lambda)_{max}$ (Å^{-1})	0.691	0.675
Refinement		
$R[F^2 > 2\sigma(F^2)]$, $wR(F^2)$, S	0.052, 0.150, 1.06	0.019, 0.044, 1.08
No. of reflections	14320	10196
No. of parameters	741	529
No. of restraints	501	0
	$w = 1/[\sigma^2(F_o^2) + (0.0752P)^2 + 26.4639P]$ where $P = (F_o^2 + 2F_c^2)/3$	$w = 1/[\sigma^2(F_o^2) + (0.0202P)^2 + 1.5222P]$ where $P = (F_o^2 + 2F_c^2)/3$
$\Delta\rho_{max}$, $\Delta\rho_{min}$ (e Å^{-3})	2.12, -1.83	0.63, -0.40
Absolute structure		Refined as an inversion twin.
Absolute structure parameter		0.491 (4)

Computer programs: Bruker *APEX2*, Bruker *SAINT*, *SHELXS97* (Sheldrick 2008), *SHELXL2014*/7 (Sheldrick, 2014), Bruker *SHELXTL*.

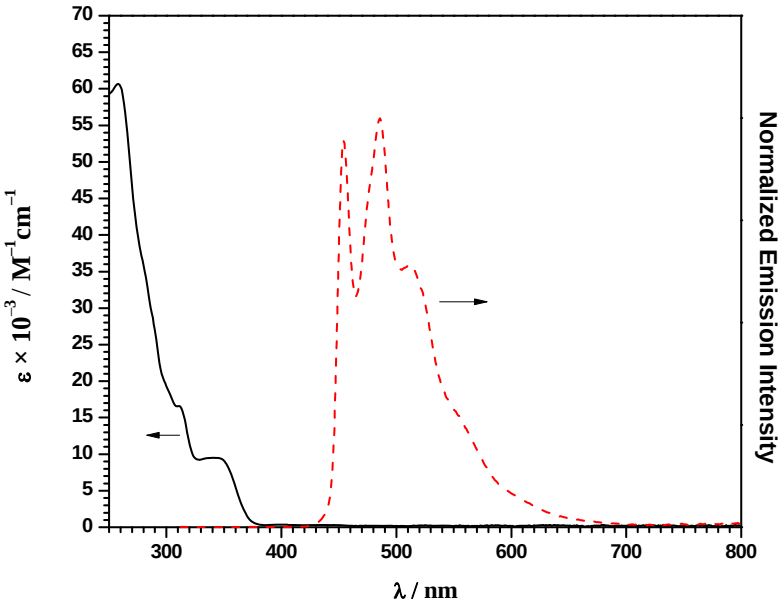

Figure S1. UV-vis absorption (**—**, black) and emission (---, red) spectra of **1a**, $[Ir(ppy)_2(CNAr^{dmp})_2]PF_6$, measured at room temperature in DCM solution.

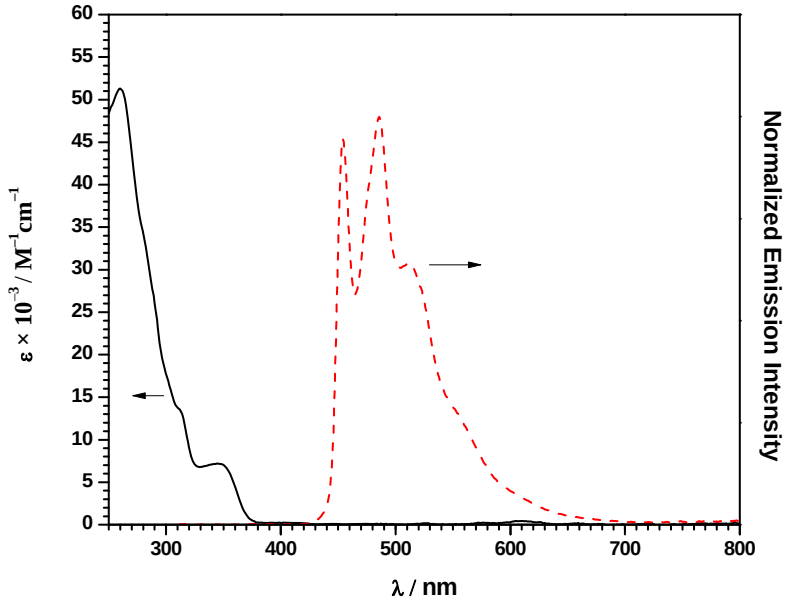

Figure S2. UV-vis absorption (**—**, black) and emission (---, red) spectra of **1b**. $[Ir(ppy)_2(CNAr^{dipp})_2]PF_6$ measured at room temperature in DCM solution.

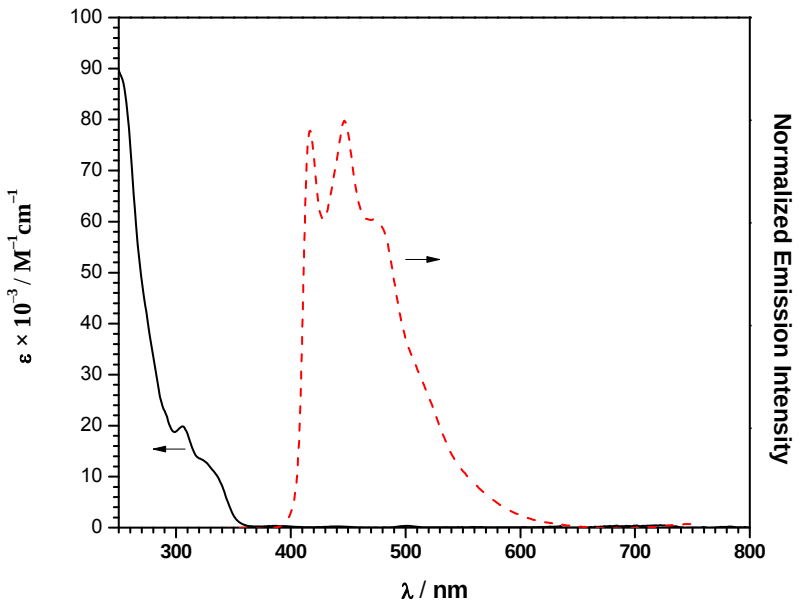

Figure S3. UV-vis absorption (**—**, black) and emission (---, red) spectra of **2a,** $[Ir(F_2ppy)_2(CNAr^{dmp})_2]PF_6$ measured at room temperature in DCM solution.

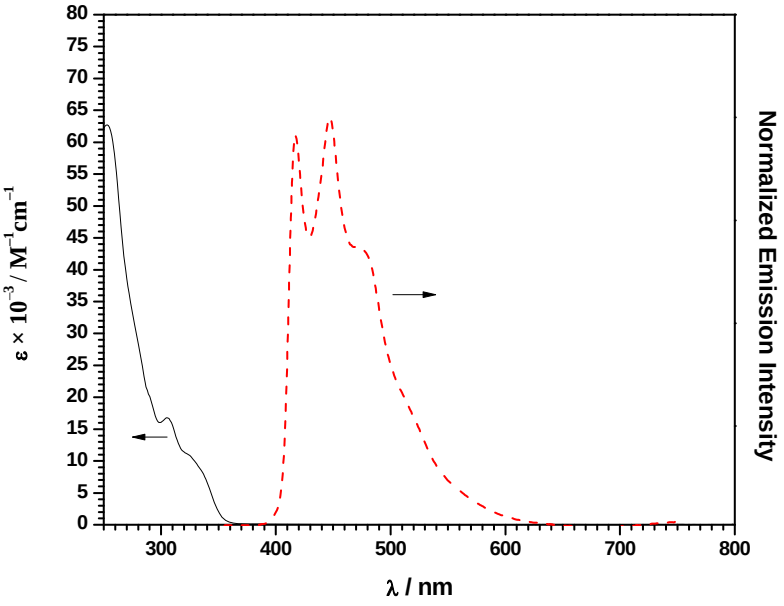

Figure S4. UV-vis absorption (**—**, black) and emission (---, red) spectra of **2b,** $[Ir(F_2ppy)_2(CNAr^{dipp})_2]PF_6$ measured at room temperature in DCM solution.

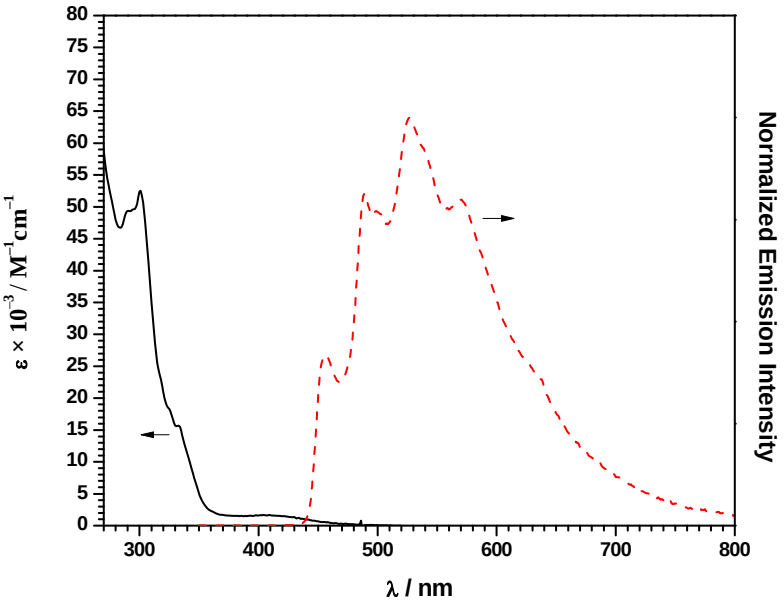

Figure S5. UV-vis absorption (**—**, black) and emission (---, red) spectra of **2c,** $[Ir(F_2ppy)_2(CNAr^{nap})_2]PF_6$ measured at room temperature in DCM solution.

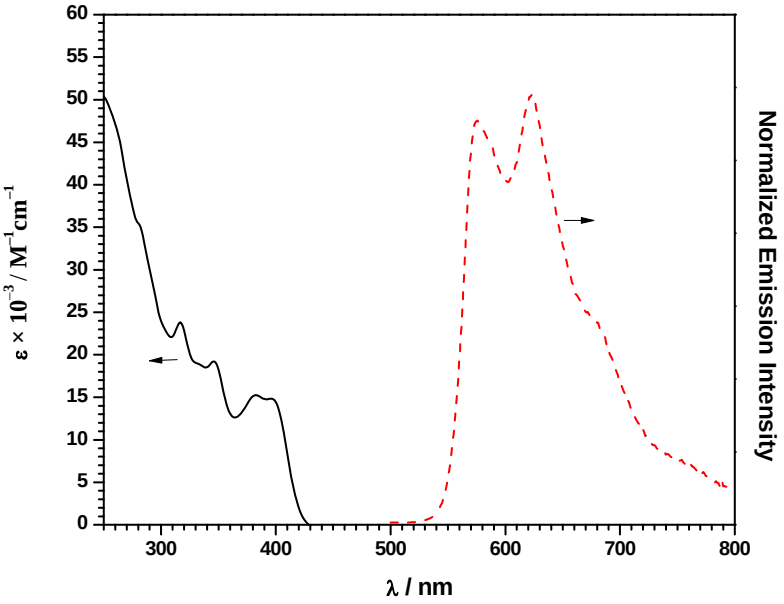

Figure S6. UV-vis absorption (**—**, black) and emission (---, red) spectra of **3a,** $[Ir(btp)_2(CNAr^{dmp})_2]PF_6$ measured at room temperature in DCM solution.

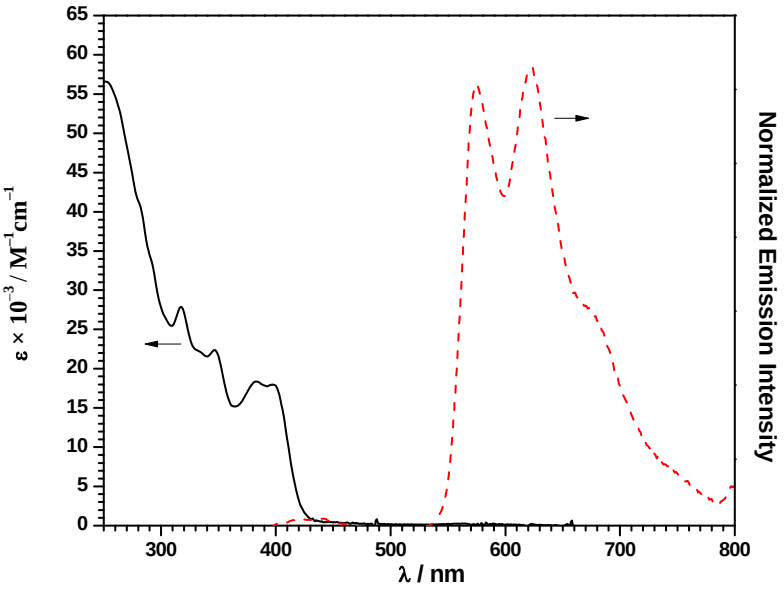

Figure S7. UV-vis absorption (▬, black) and emission (---, red) spectra of **3b,** $[Ir(btp)_2(CNAr^{dipp})_2]PF_6$ measured at room temperature in DCM solution.

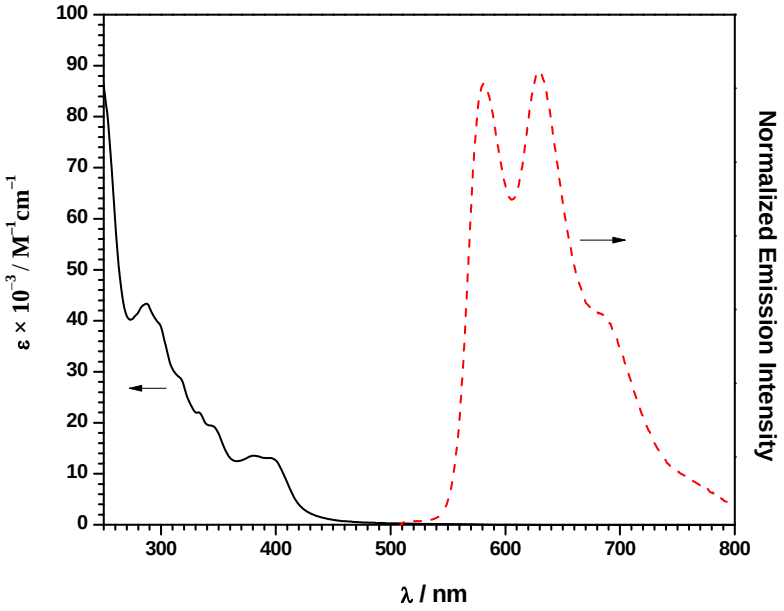

Figure S8. UV-vis absorption (▬, black) and emission (---, red) spectra of **3c,** $[Ir(btp)_2(CNAr^{nap})_2]PF_6$ measured at room temperature in DCM solution.

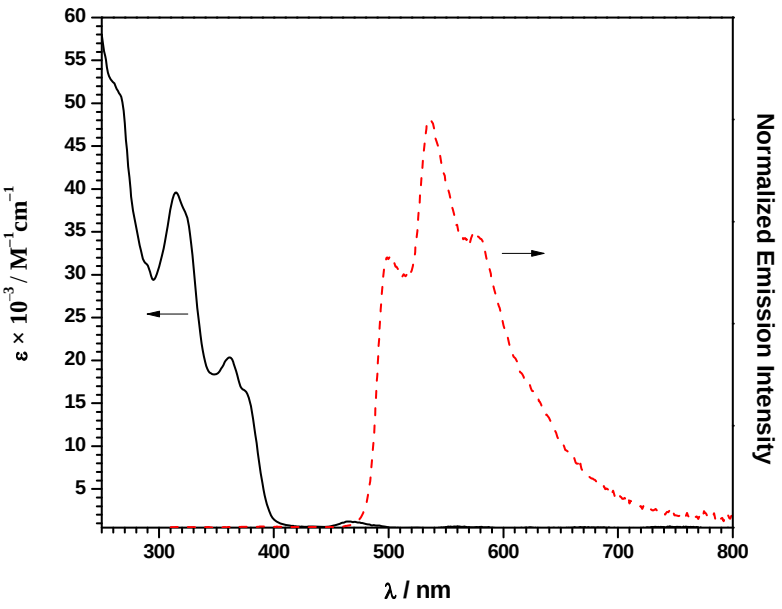

Figure S9. UV-vis absorption (**—**, black) and emission (---, red) spectra of **4a,** $[Ir(bt)_2(CNAr^{dmp})_2]PF_6$ measured at room temperature in DCM solution.

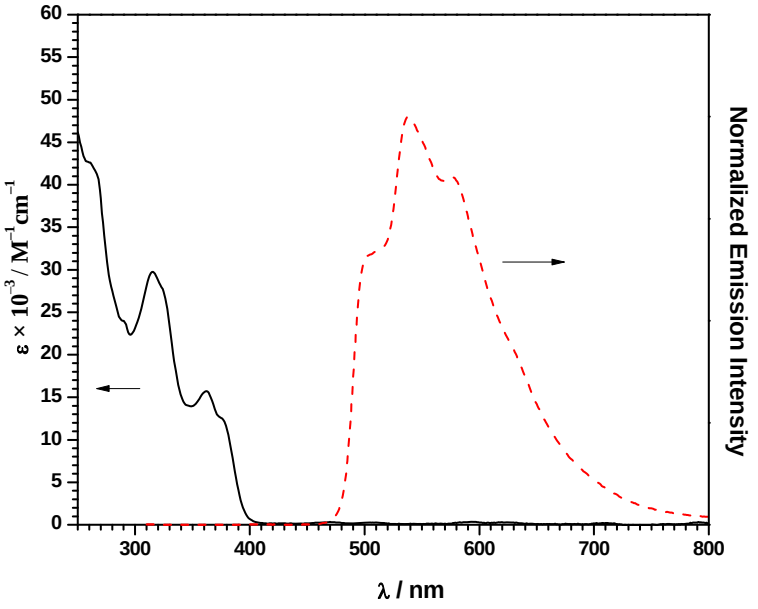

Figure S10. UV-vis absorption (**—**, black) and emission (---, red) spectra of **4b,** $[Ir(bt)_2(CNAr^{dipp})_2]PF_6$ measured at room temperature in DCM solution.

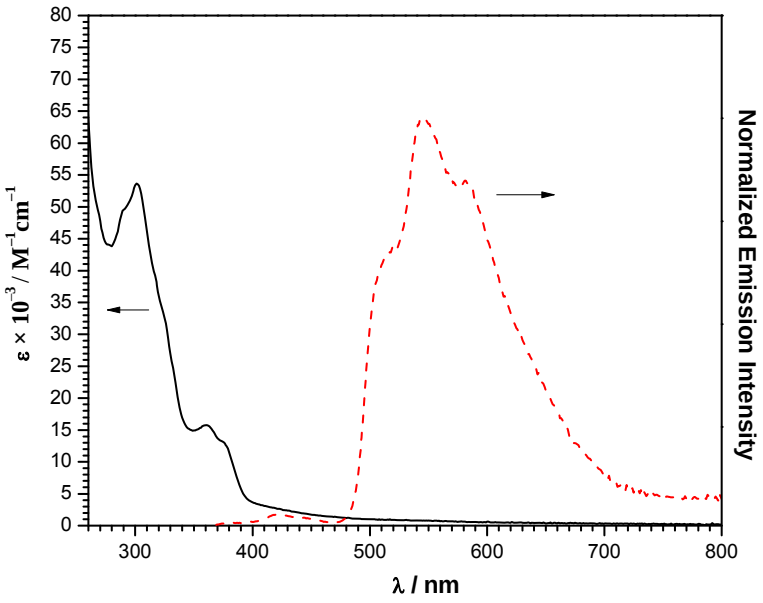

Figure S11. UV-vis absorption (**—**, black) and emission (---, red) spectra of **4c,** $[Ir(bt)_2(CNAr^{nap})_2]PF_6$ measured at room temperature in DCM solution.

Cyclic voltammetry experiments. All redox processes were irreversible. Relative to Fc^+/Fc. The CVs were performed in acetonitrile with 0.1 M NBu_4PF_6 electrolyte using a glassy carbon working electrode and a scan rate of 0.1 V/s. Currents are normalized to put the individual traces on the same scale, and the arrows show approximate starting potentials and scan direction.

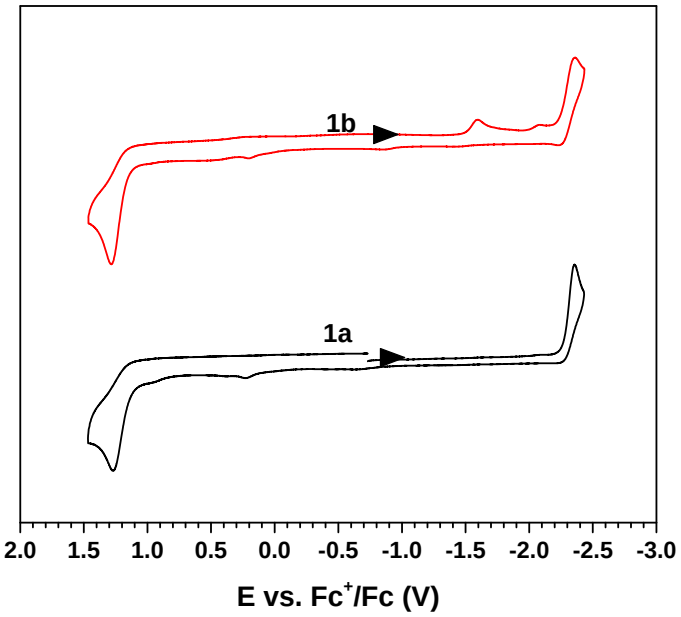

Figure S12. Overlaid cyclic voltammograms of **1a–b**.

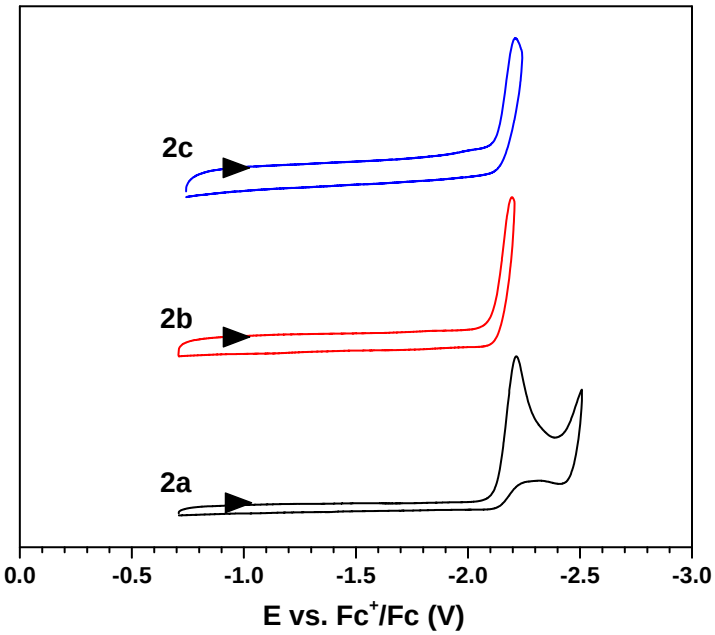

Figure S13. Overlaid cyclic voltammograms of **2a–c**.

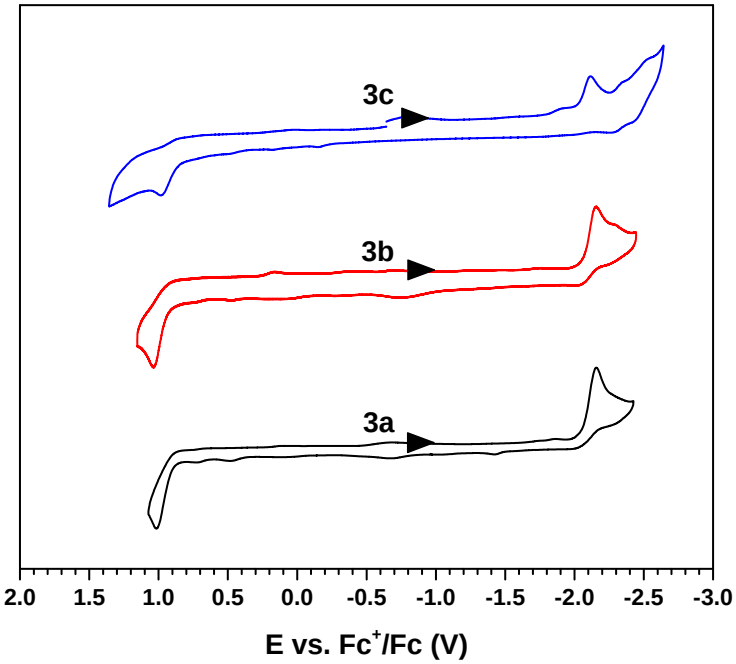

Figure S14. Overlaid cyclic voltammograms of **3a–c**.

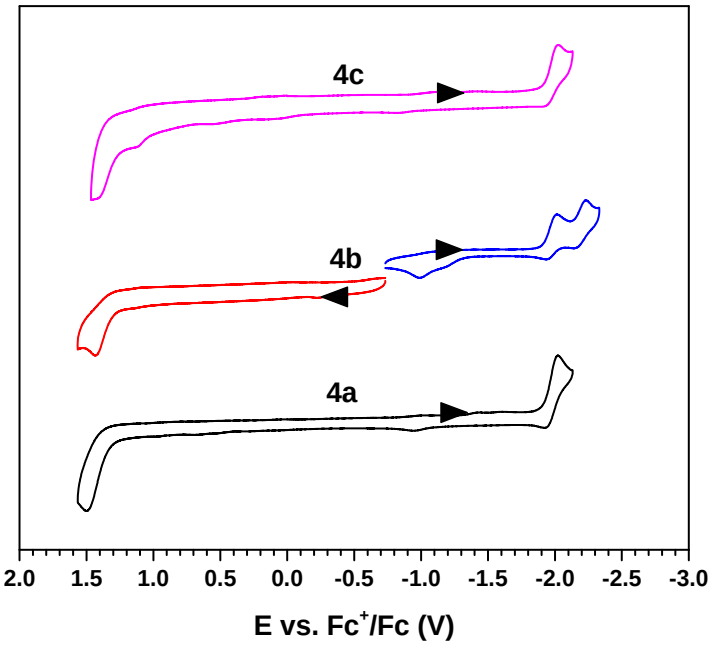

Figure S15. Overlaid cyclic voltammograms of **4a–c**.

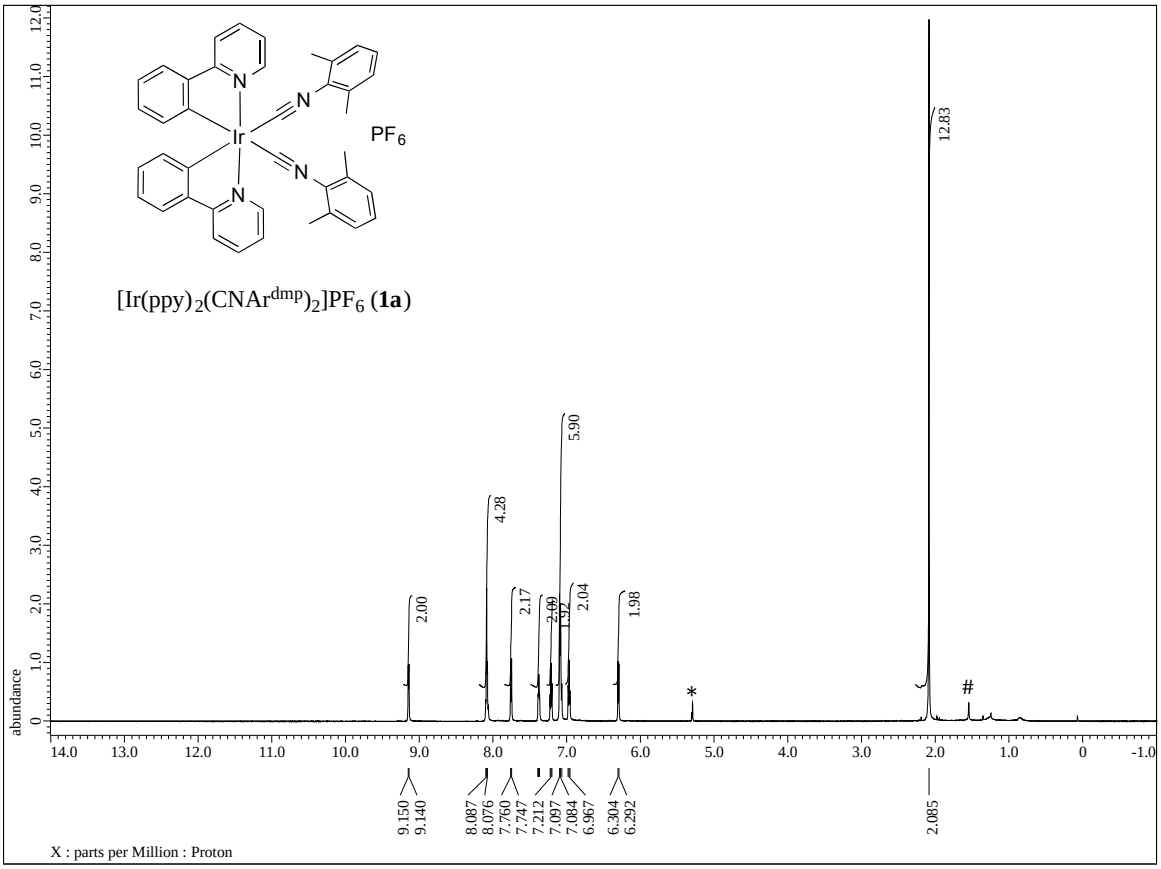

Figure S16. ^{1}H NMR spectrum of $[Ir(ppy)_2(CNAr^{dmp})_2]PF_6$ (**1a**), recorded at 600 MHz in $CDCl_3$. Residual solvent peaks for dichloromethane (*) and water (#) are marked accordingly.

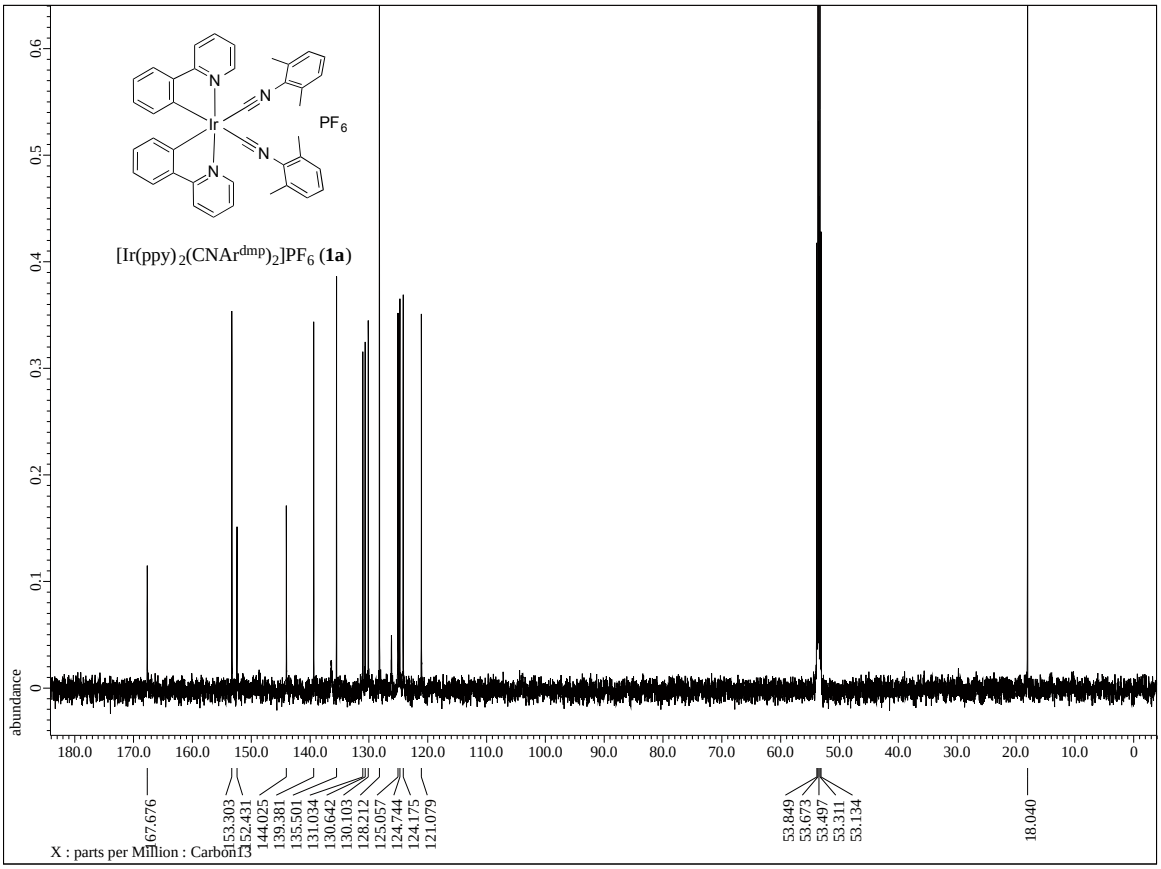

Figure S17. $^{13}C\{^{1}H\}$ NMR spectrum of $[Ir(ppy)_2(CNAr^{dmp})_2]PF_6$ (**1a**), recorded at 151 MHz in CD_2Cl_2.

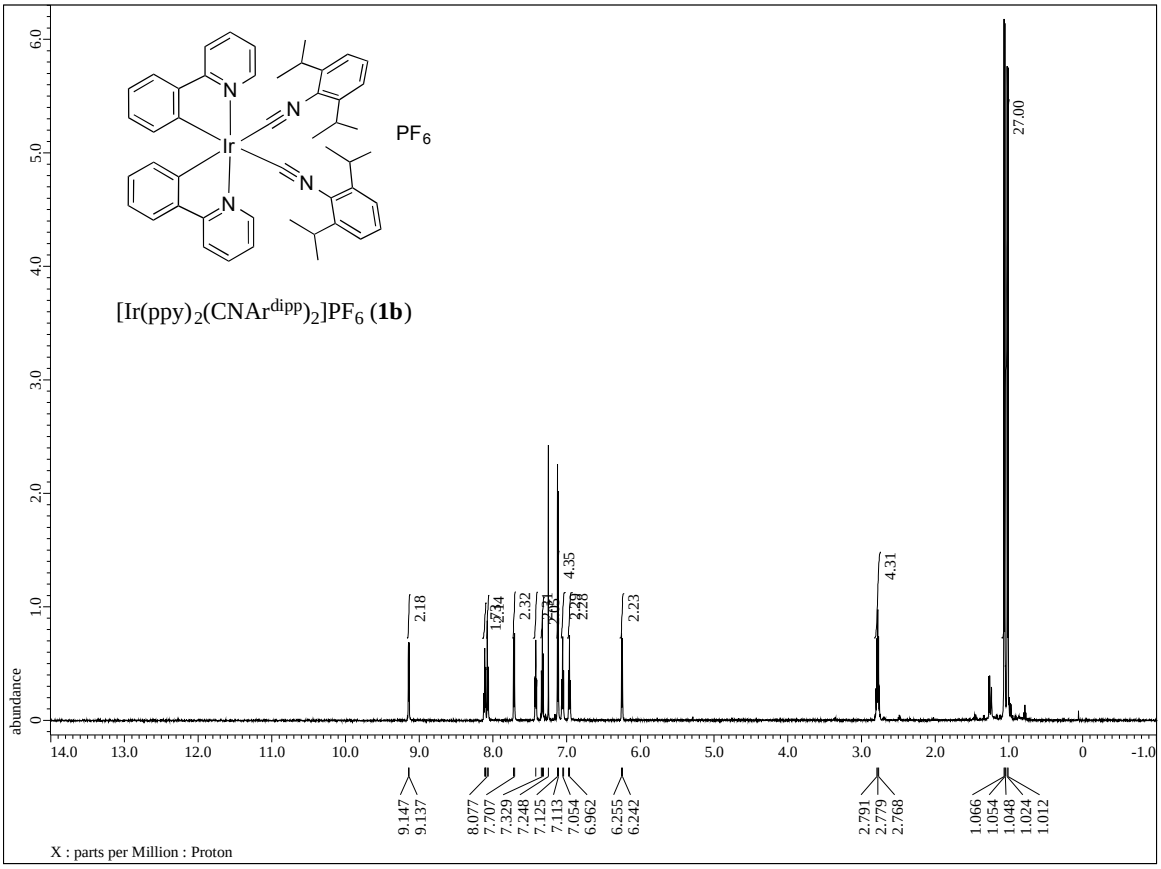

Figure S18. ^{1}H NMR spectrum of $[Ir(ppy)_2(CNAr^{dipp})_2]PF_6$ (**1b**), recorded at 600 MHz in $CDCl_3$.

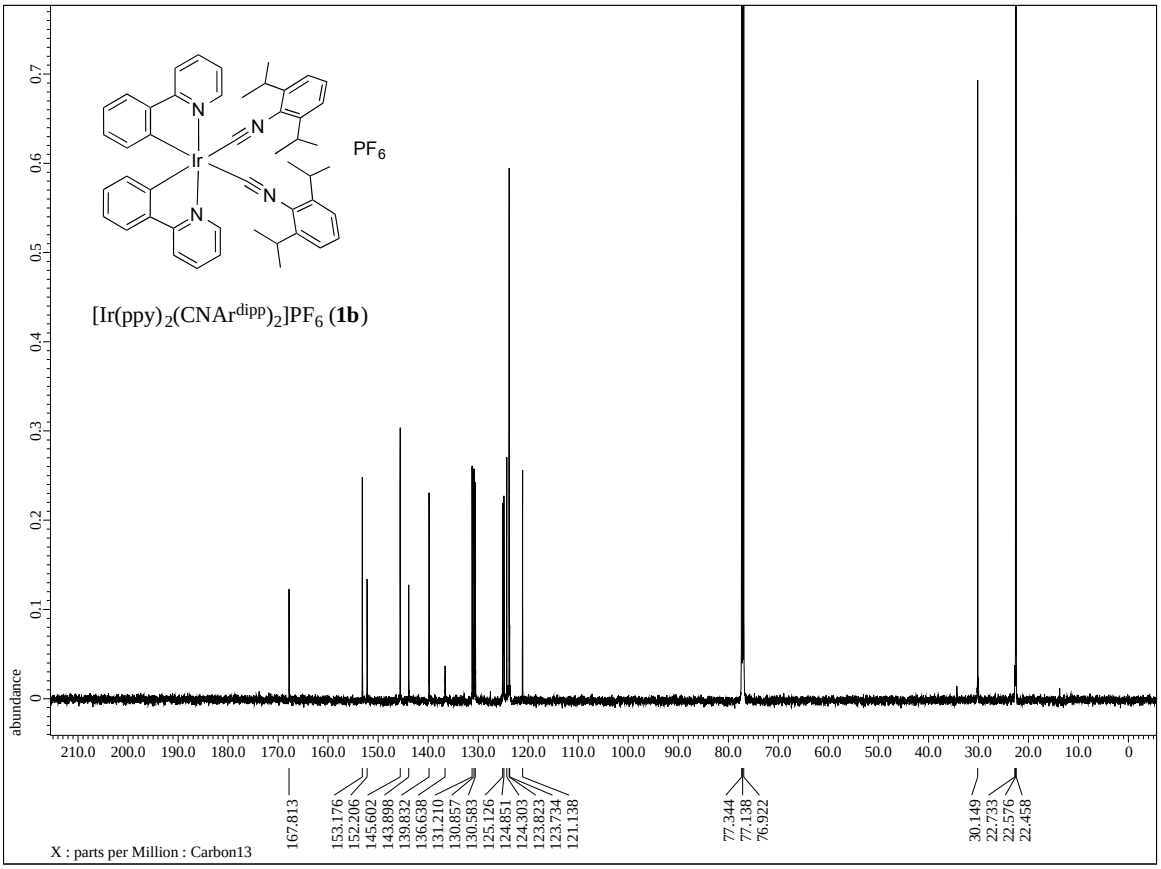

Figure S19. $^{13}C\{^{1}H\}$ NMR spectrum of $[Ir(ppy)_2(CNAr^{dipp})_2]PF_6$ (**1b**), recorded at 151 MHz in $CDCl_3$.

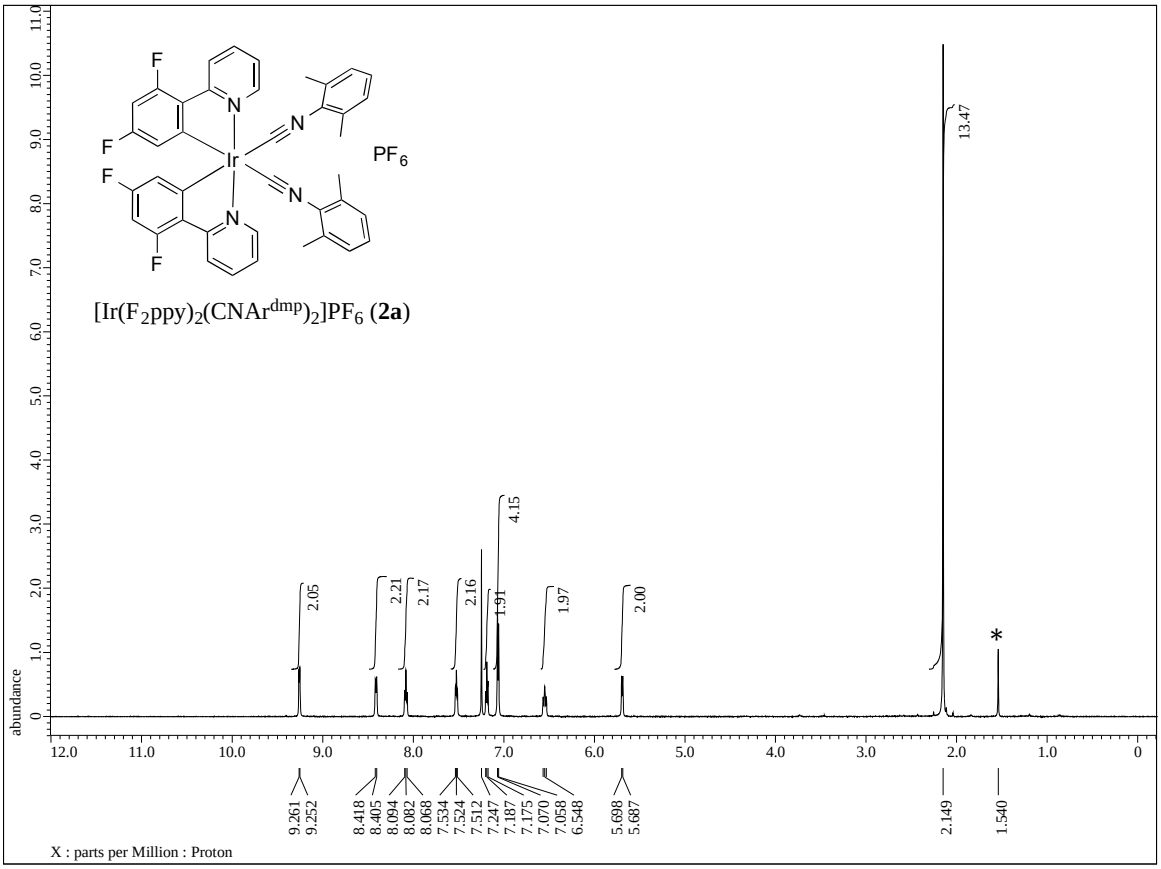

Figure S20. ^{1}H NMR spectrum of $[Ir(F_2ppy)_2(CNAr^{dmp})_2]PF_6$ (**2a**), recorded at 600 MHz in $CDCl_3$. Residual solvent peak for water (*) is marked.

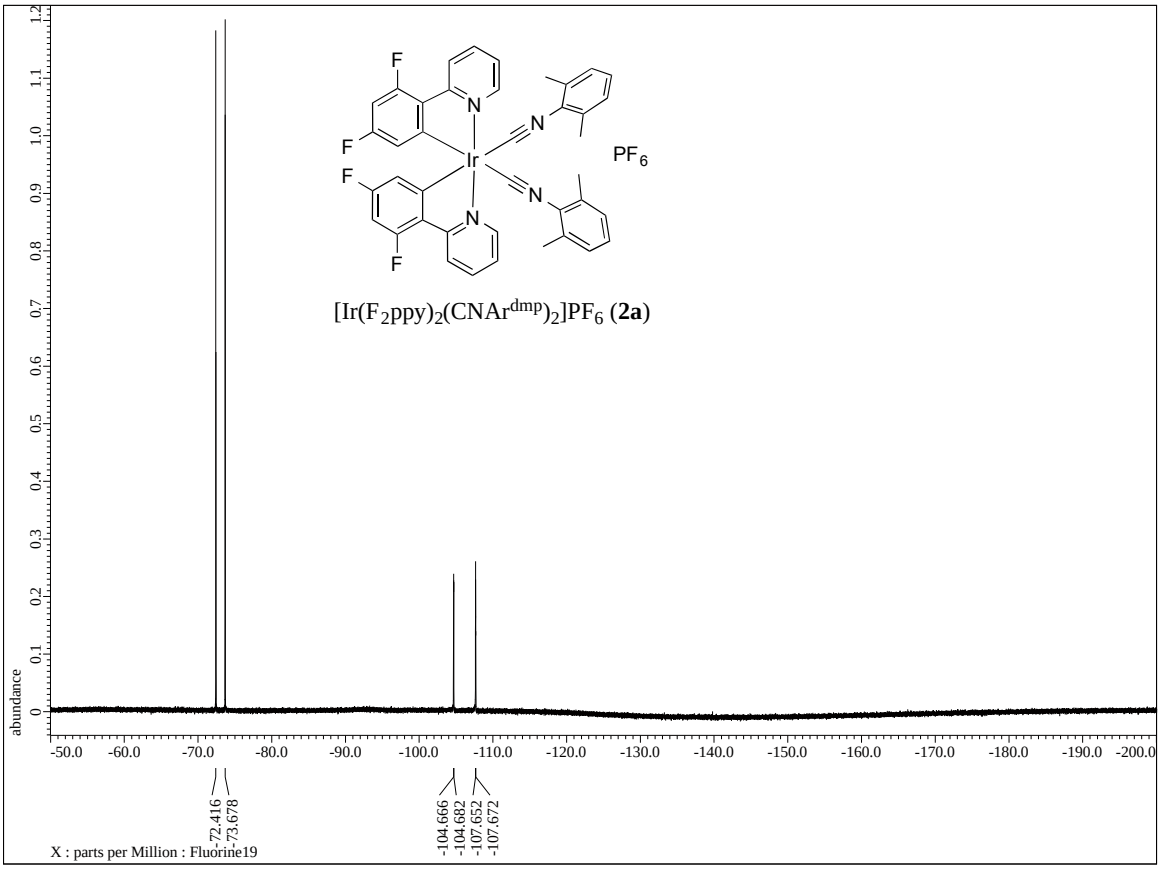

Figure S21. ^{19}F NMR spectrum of $[Ir(F_2ppy)_2(CNAr^{dmp})_2]PF_6$ (**2a**), recorded at 565 MHz in $CDCl_3$.

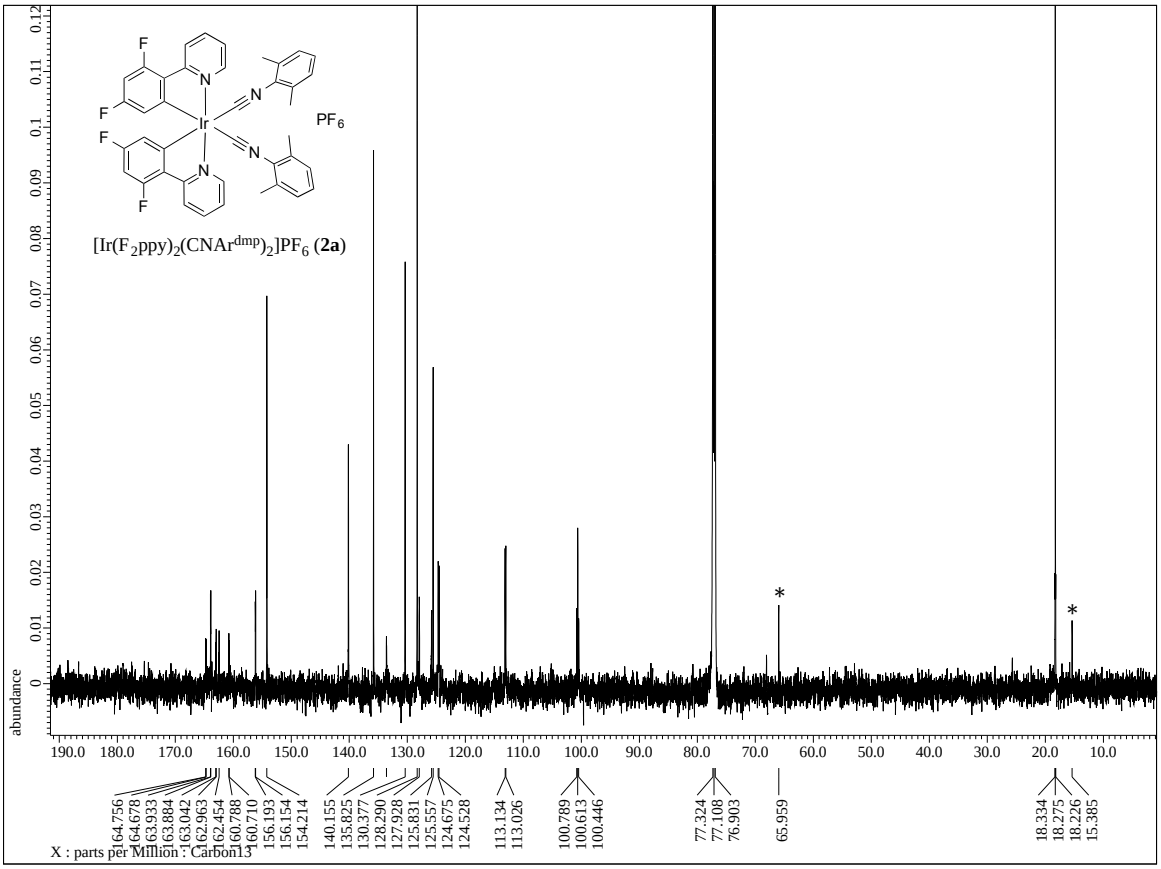

Figure S22. $^{13}C\{^{1}H\}$ NMR spectrum of $[Ir(F_2ppy)_2(CNAr^{dmp})_2]PF_6$ (**2a**), recorded at 151 MHz in $CDCl_3$. Residual solvent peaks for diethyl ether (*) are marked.

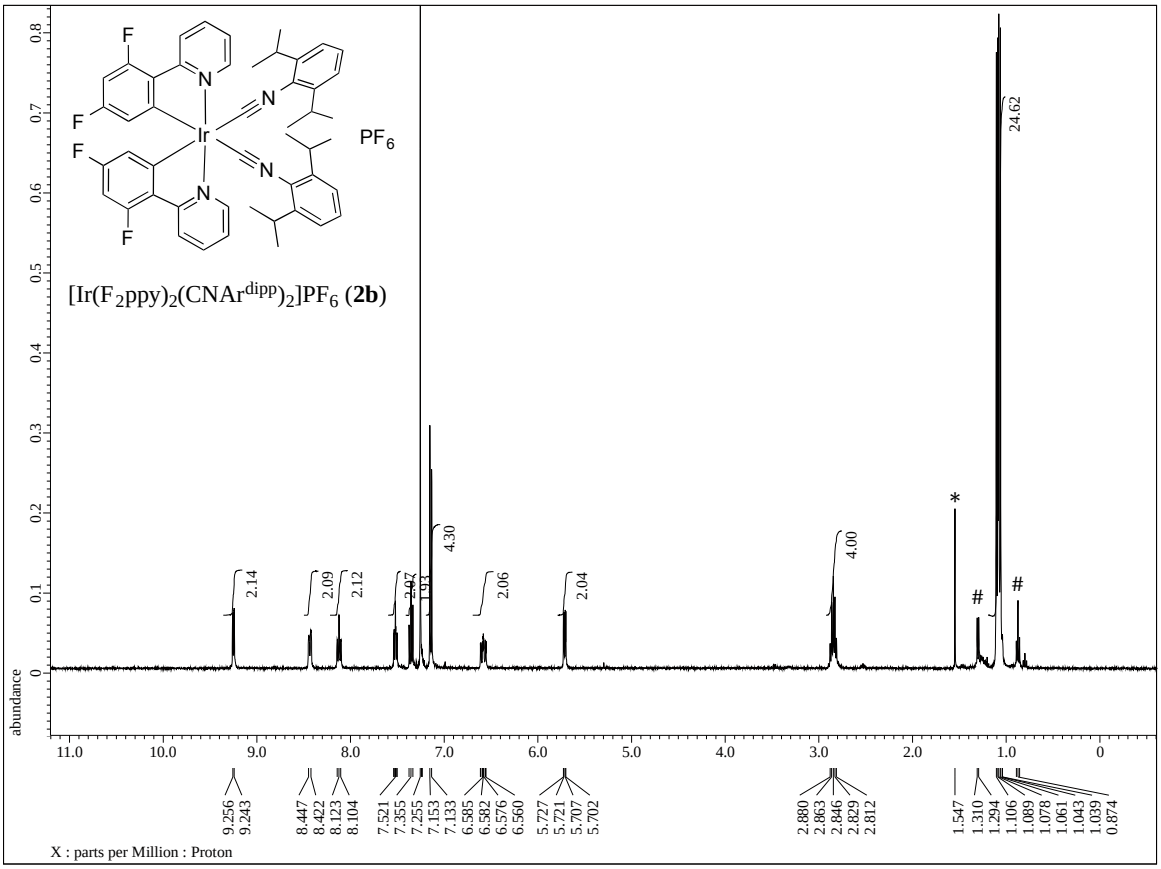

Figure S23. ^{1}H NMR spectrum of $[Ir(F_2ppy)_2(CNAr^{dipp})_2]PF_6$ (**2b**), recorded at 600 MHz in $CDCl_3$. Residual solvent peaks for water (*) and pentane (#) are marked accordingly.

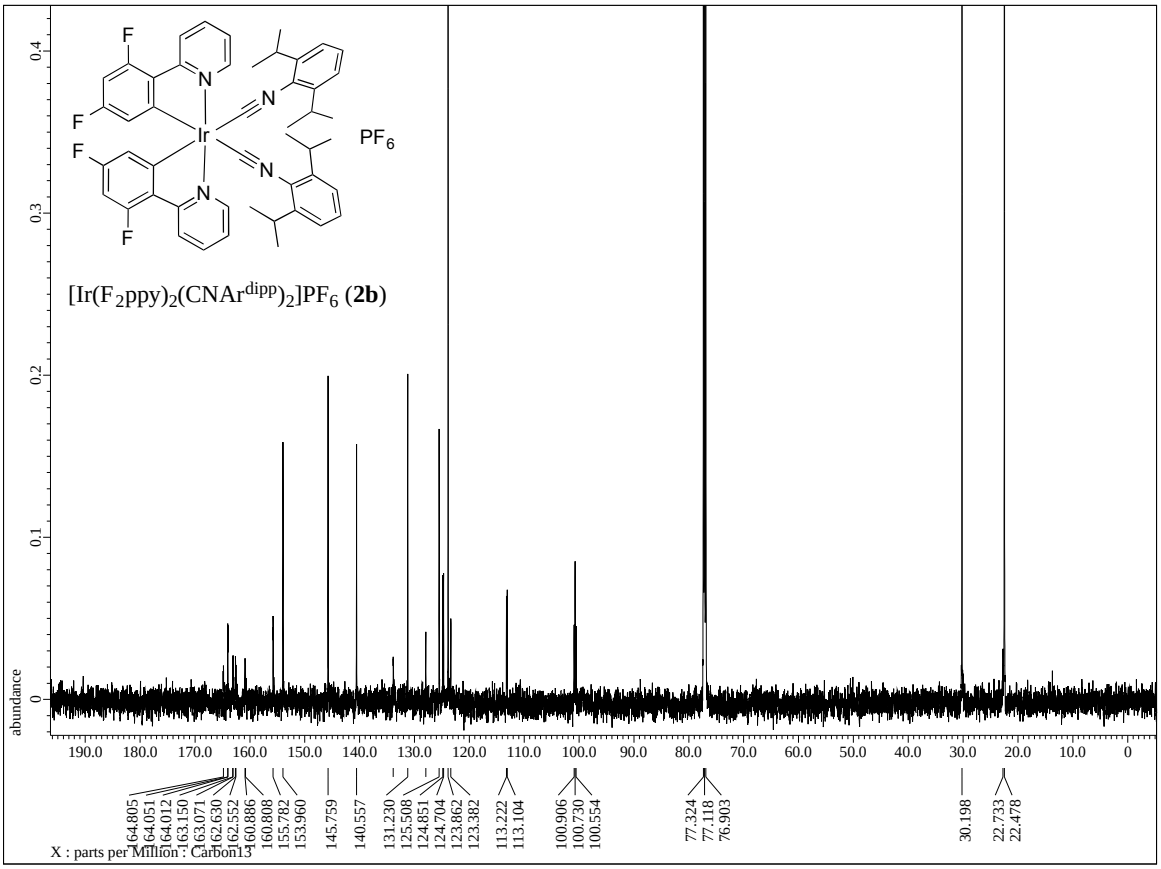

Figure S24. $^{13}C\{^{1}H\}$ NMR spectrum of $[Ir(F_2ppy)_2(CNAr^{dipp})_2]PF_6$ (**2b**), recorded at 151 MHz in $CDCl_3$.

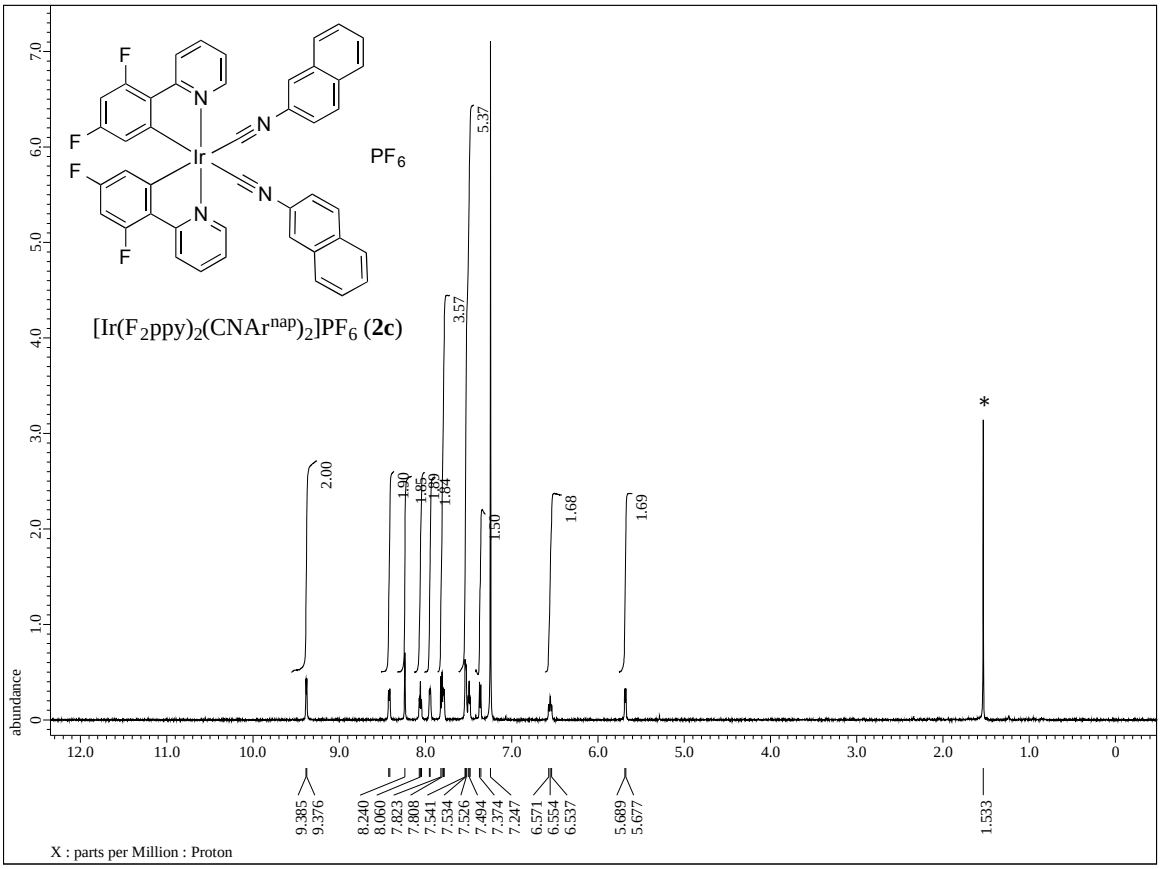

Figure S25. ^{1}H NMR spectrum of $[Ir(F_2ppy)_2(CNAr^{nap})_2]PF_6$ (**2c**), recorded at 600 MHz in $CDCl_3$. Residual solvent peak for water (*) is marked.

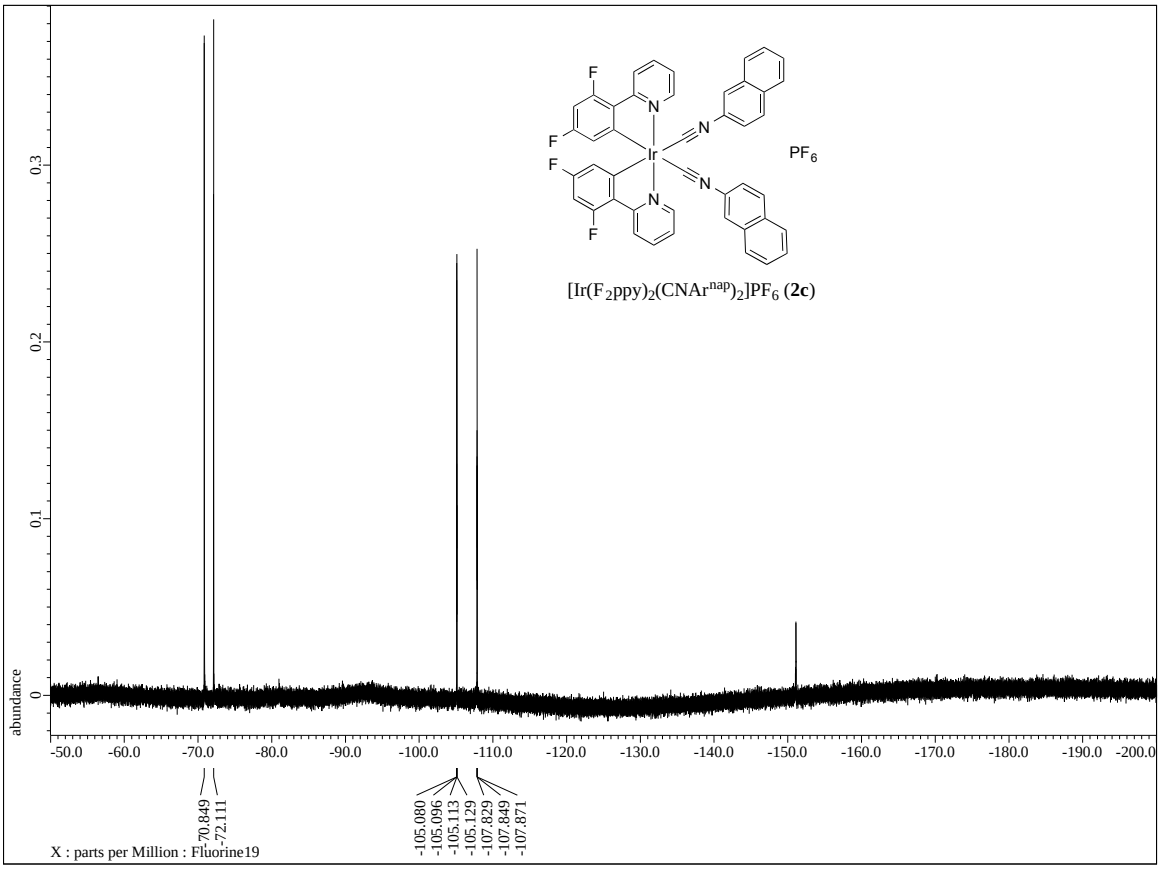

Figure S26. ^{19}F NMR spectrum of $[Ir(F_2ppy)_2(CNAr^{nap})_2]PF_6$ (**2c**), recorded at 565 MHz in $CDCl_3$.

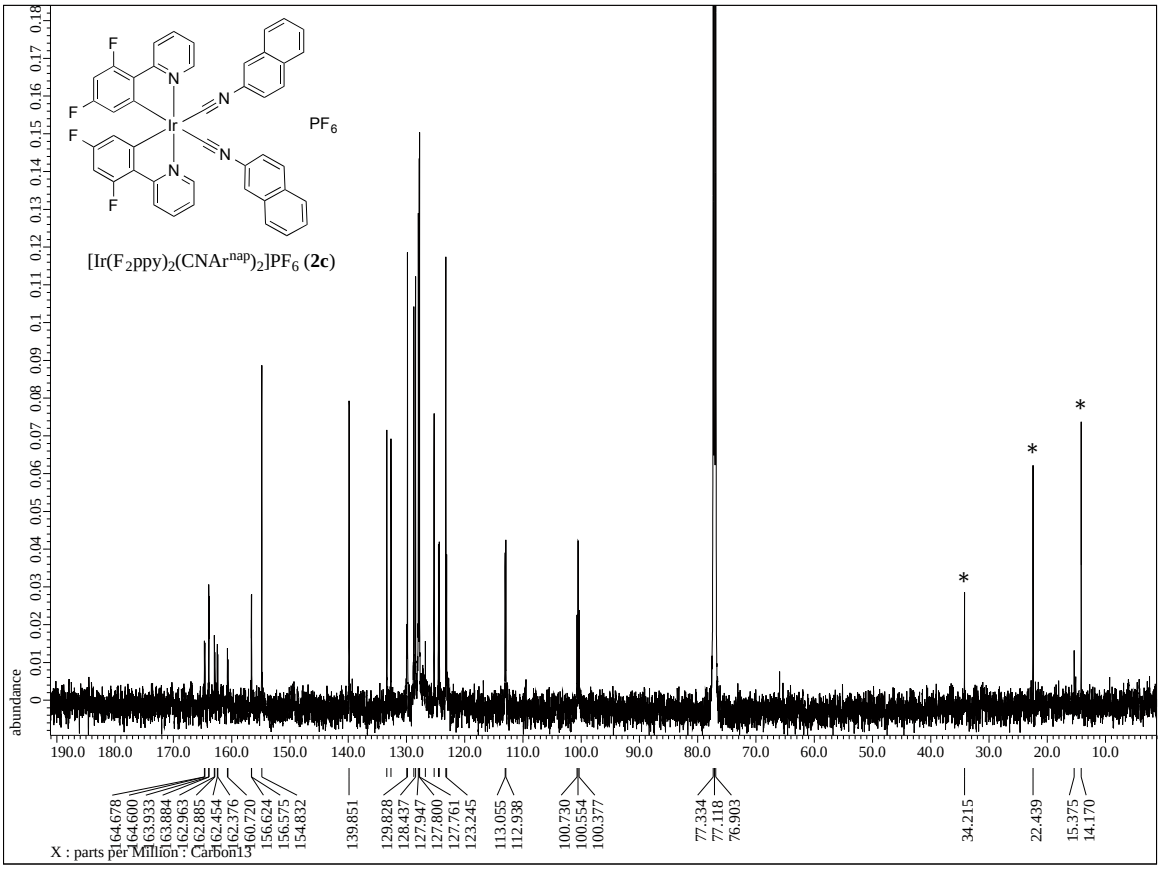

Figure S27. $^{13}C\{^{1}H\}$ NMR spectrum of $[Ir(F_2ppy)_2(CNAr^{nap})_2]PF_6$ (**2c**), recorded at 151 MHz in $CDCl_3$. Residual solvent peaks for pentane (*) are marked.

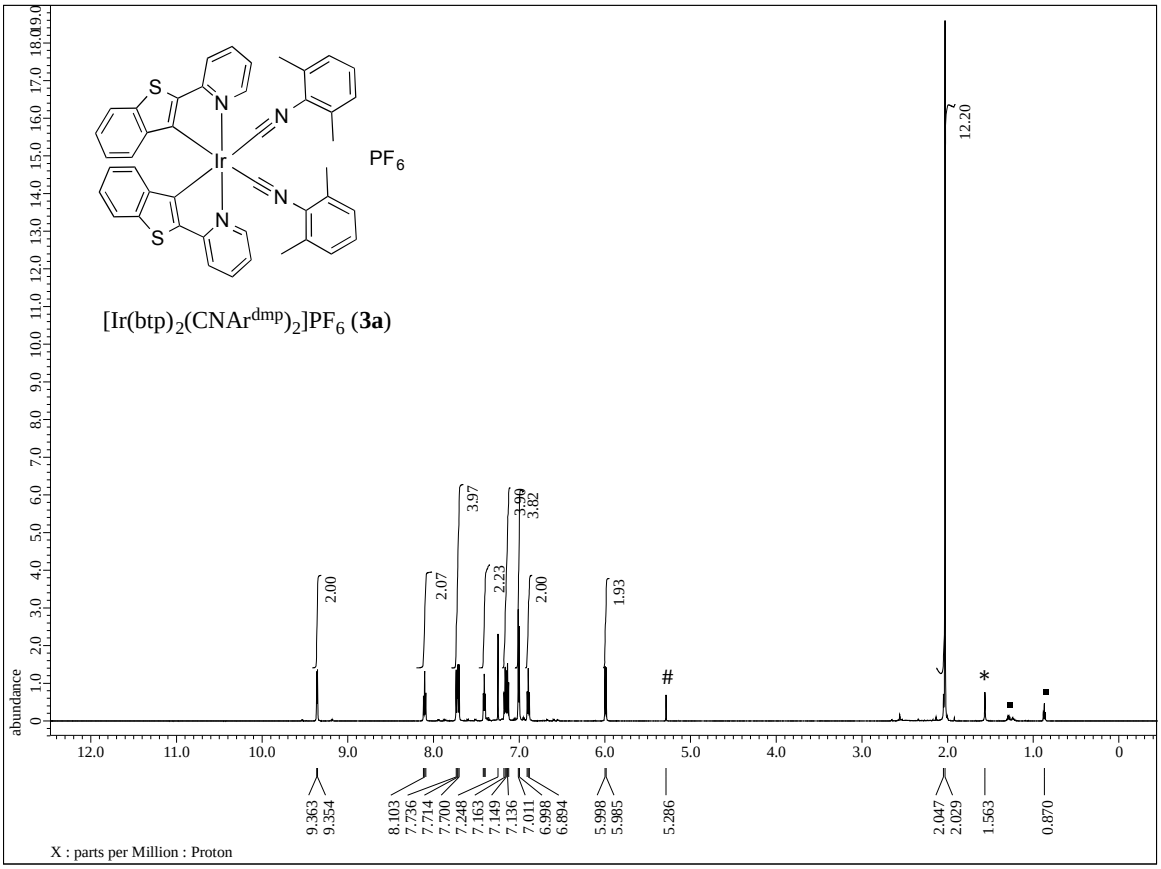

Figure S28. ^{1}H NMR spectrum of $[Ir(btp)_2(CNAr^{dmp})_2]PF_6$ (**3a**), recorded at 600 MHz in $CDCl_3$. Residual solvent peaks for CH_2Cl_2 (#), water (*) and pentane (▪) are marked accordingly.

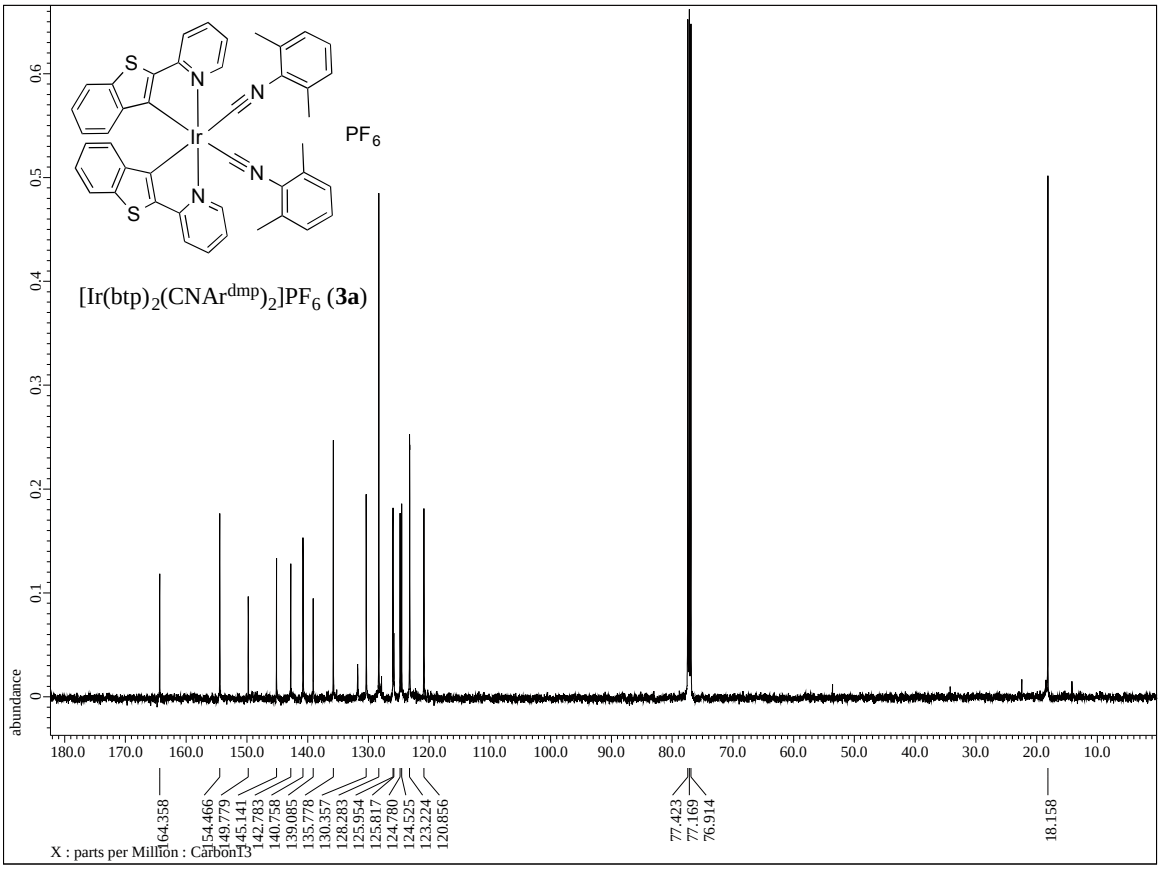

Figure S29. $^{13}C\{^{1}H\}$ NMR spectrum of $[Ir(btp)_2(CNAr^{dmp})_2]PF_6$ (**3a**), recorded at 125 MHz in $CDCl_3$.

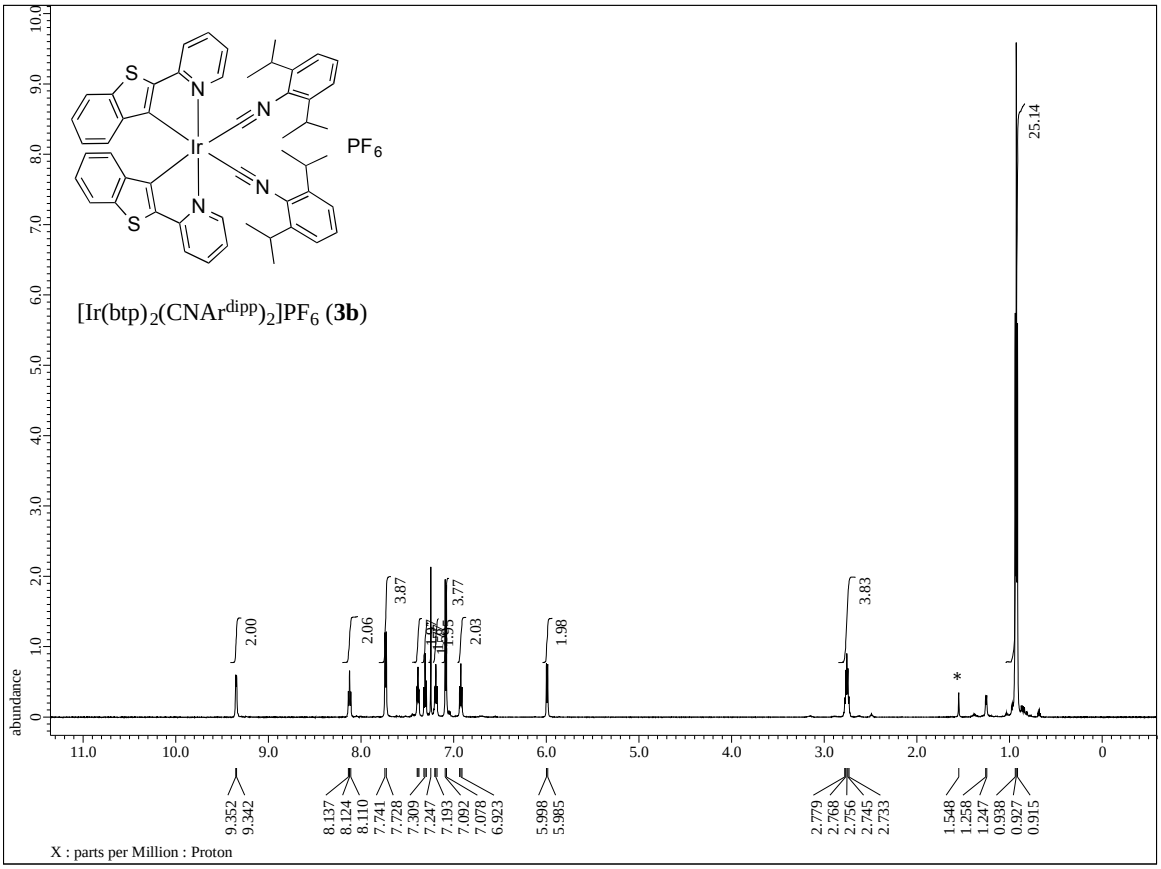

Figure S30. ^{1}H NMR spectrum of $[Ir(btp)_2(CNAr^{dipp})_2]PF_6$ (**3b**), recorded at 400 MHz in $CDCl_3$. Residual solvent peak for water (*) is marked.

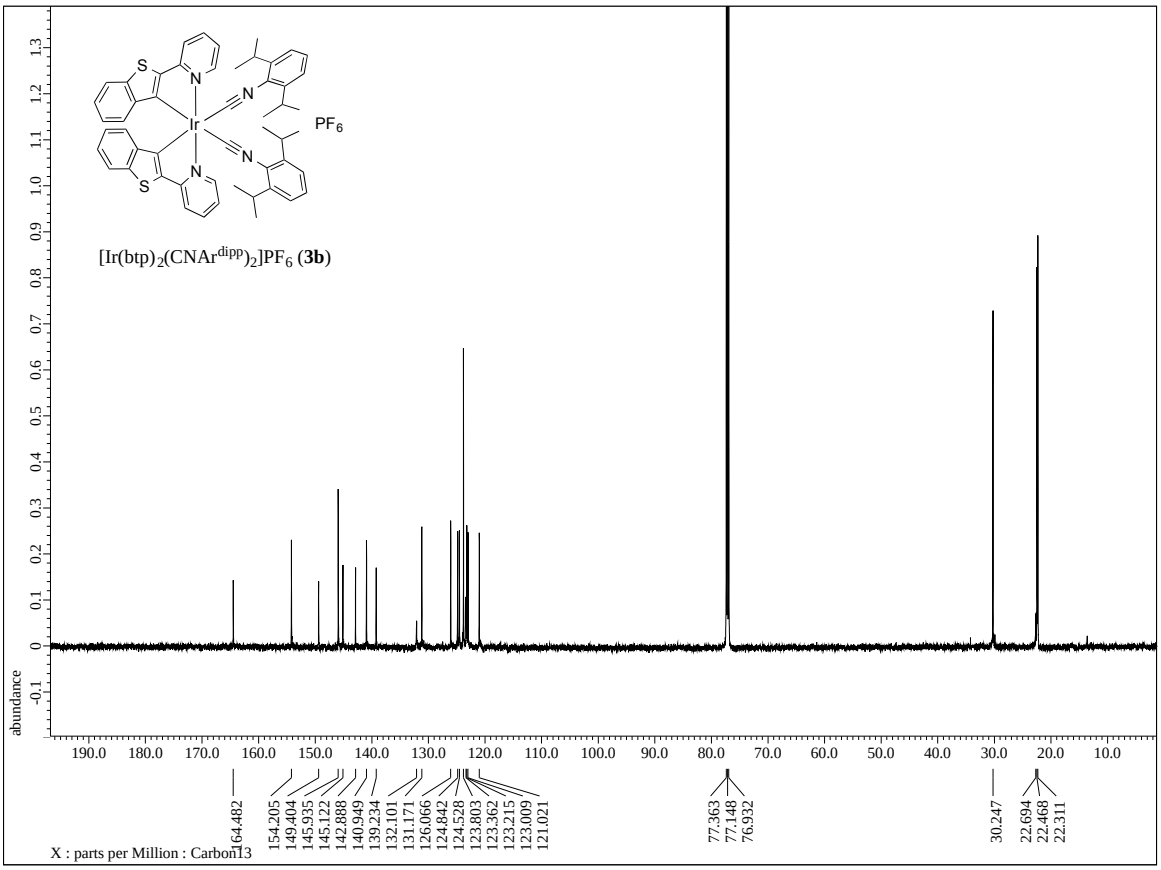

Figure S31. $^{13}C\{^{1}H\}$ NMR spectrum of $[Ir(btp)_2(CNAr^{dipp})_2]PF_6$ (**3b**), recorded at 125 MHz in $CDCl_3$.

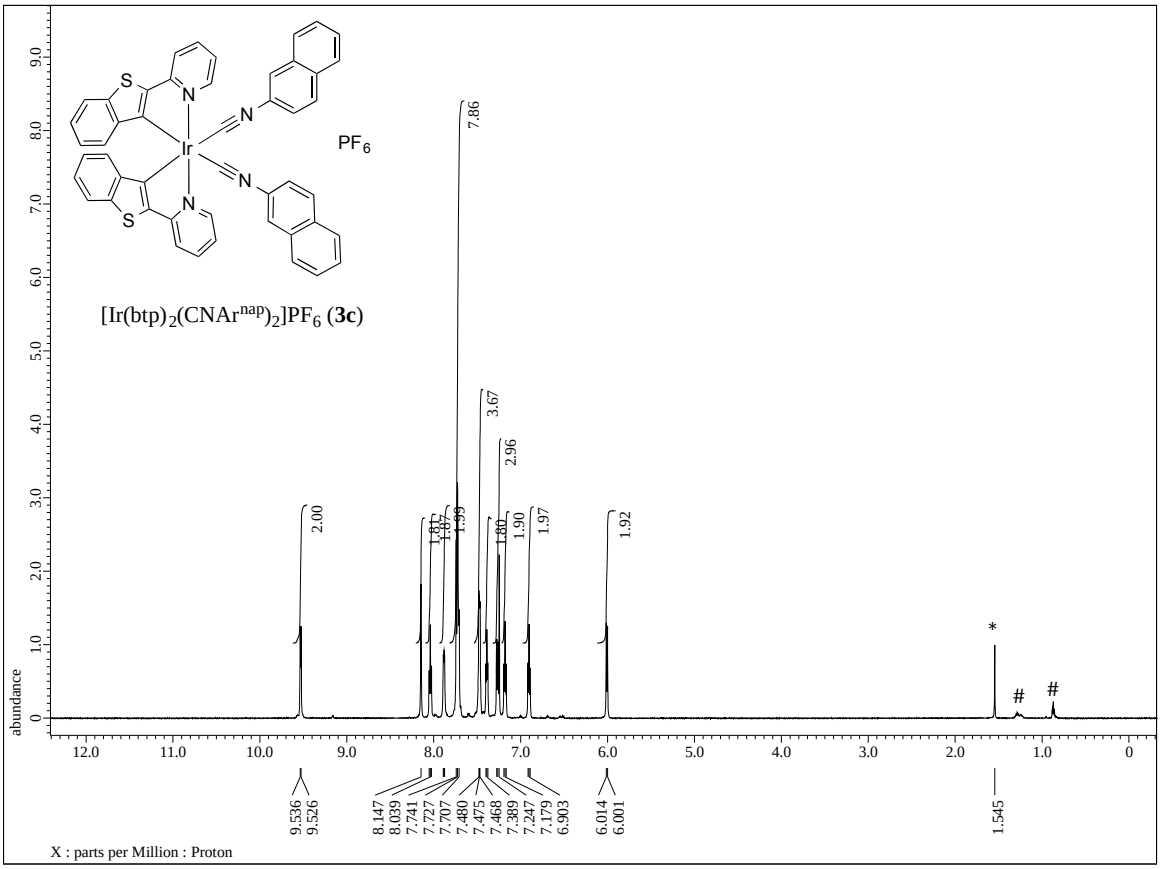

Figure S32. ^{1}H NMR spectrum of $[Ir(btp)_2(CNAr^{nap})_2]PF_6$ (**3c**), recorded at 500 MHz in $CDCl_3$. Residual solvent peaks for water (*) and pentane (#) are marked accordingly.

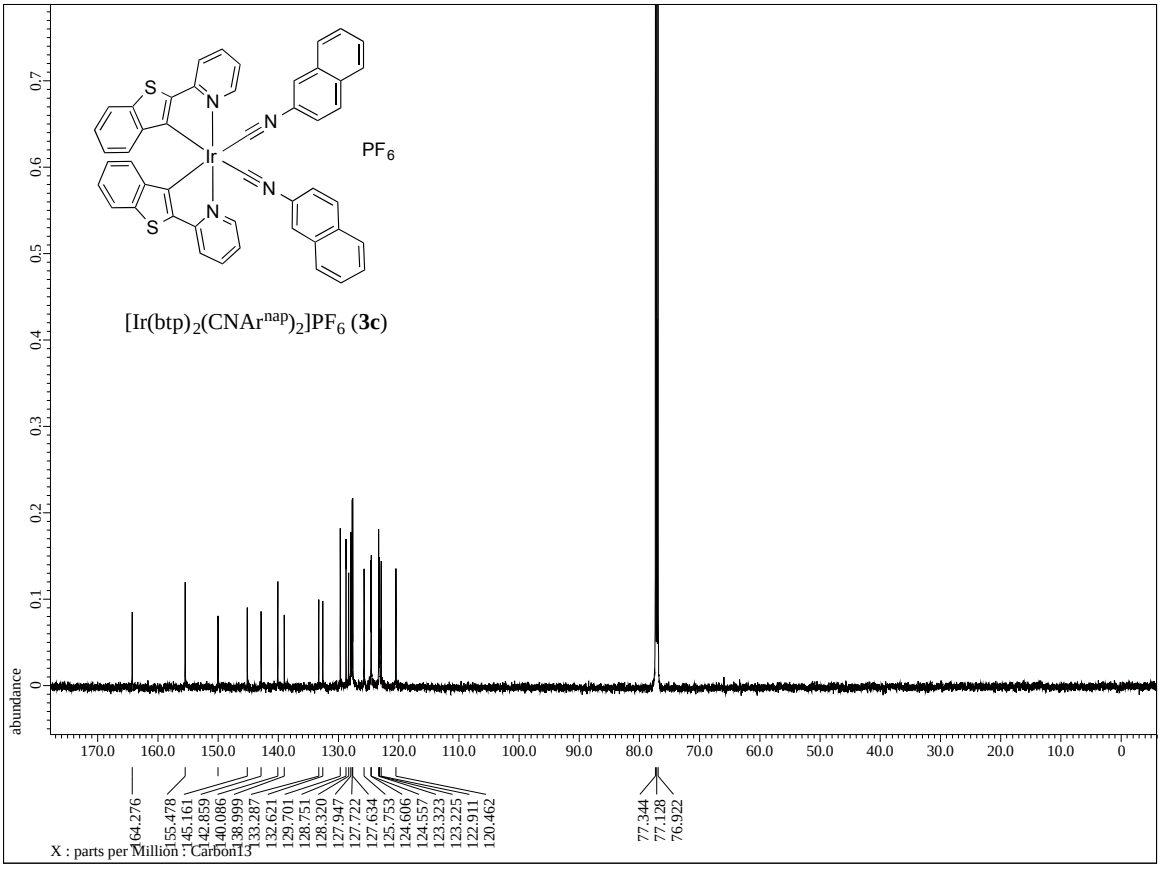

Figure S33. $^{13}C\{^{1}H\}$ NMR spectrum of $[Ir(btp)_2(CNAr^{nap})_2]PF_6$ (**3c**), recorded at 151 MHz in $CDCl_3$.

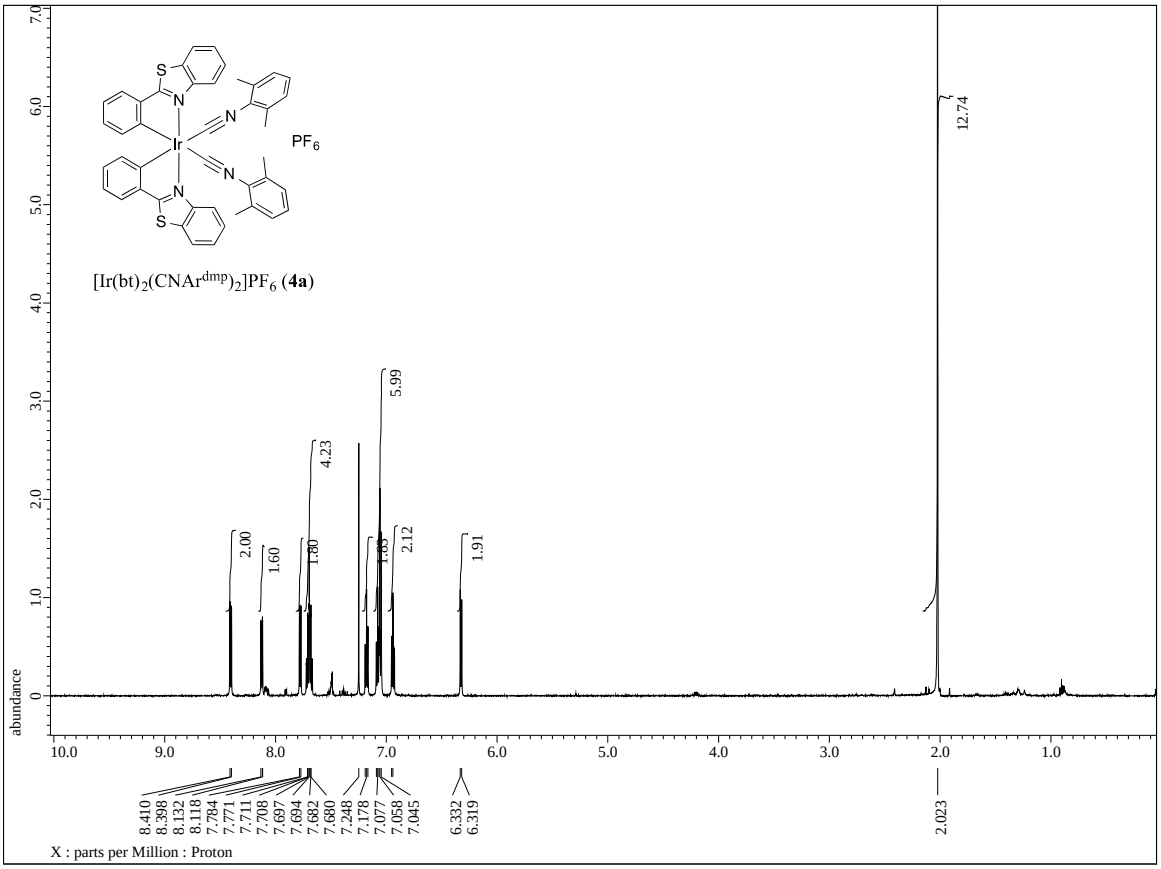

Figure S34. ^{1}H NMR spectrum of $[Ir(bt)_2(CNAr^{dmp})_2]PF_6$ (**4a**), recorded at 500 MHz in $CDCl_3$.

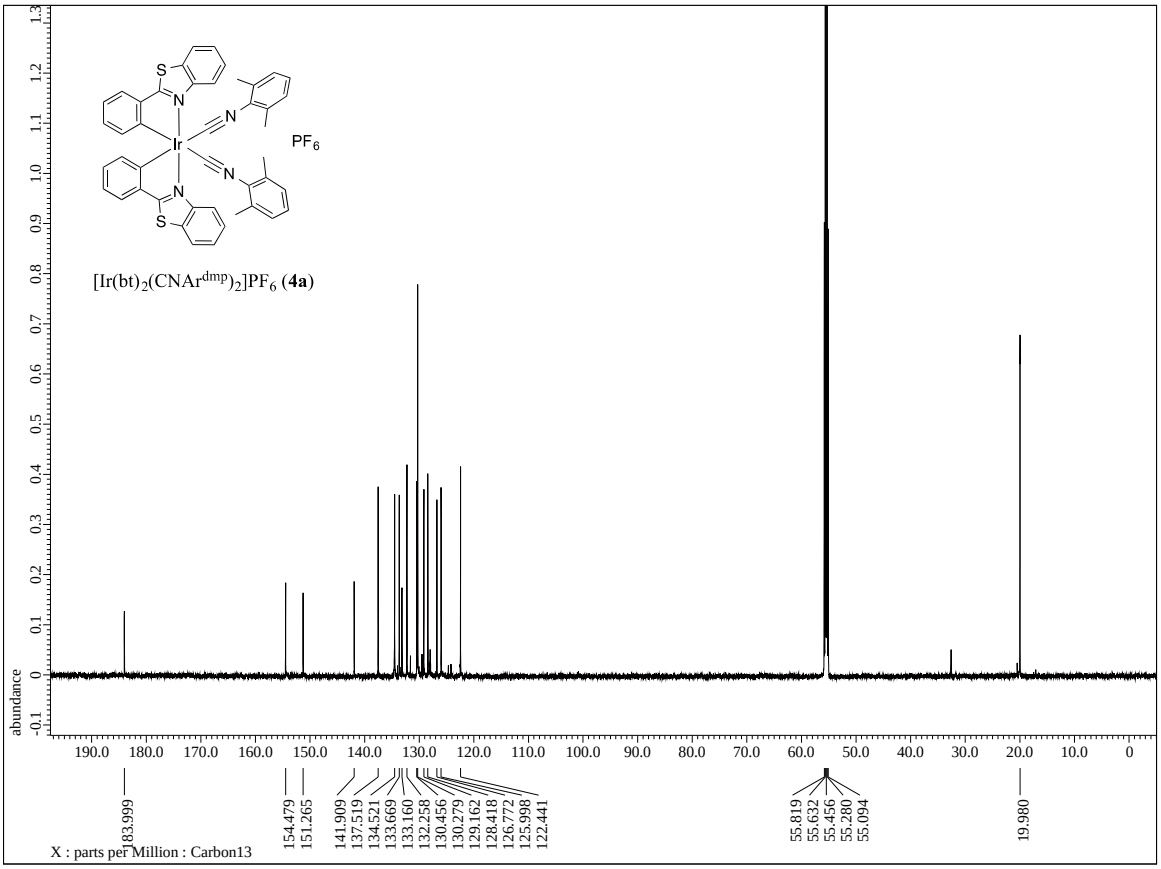

Figure S35. $^{13}C\{^{1}H\}$ NMR spectrum of $[Ir(bt)_2(CNAr^{dmp})_2]PF_6$ (**4a**), recorded at 151 MHz in $CDCl_3$.

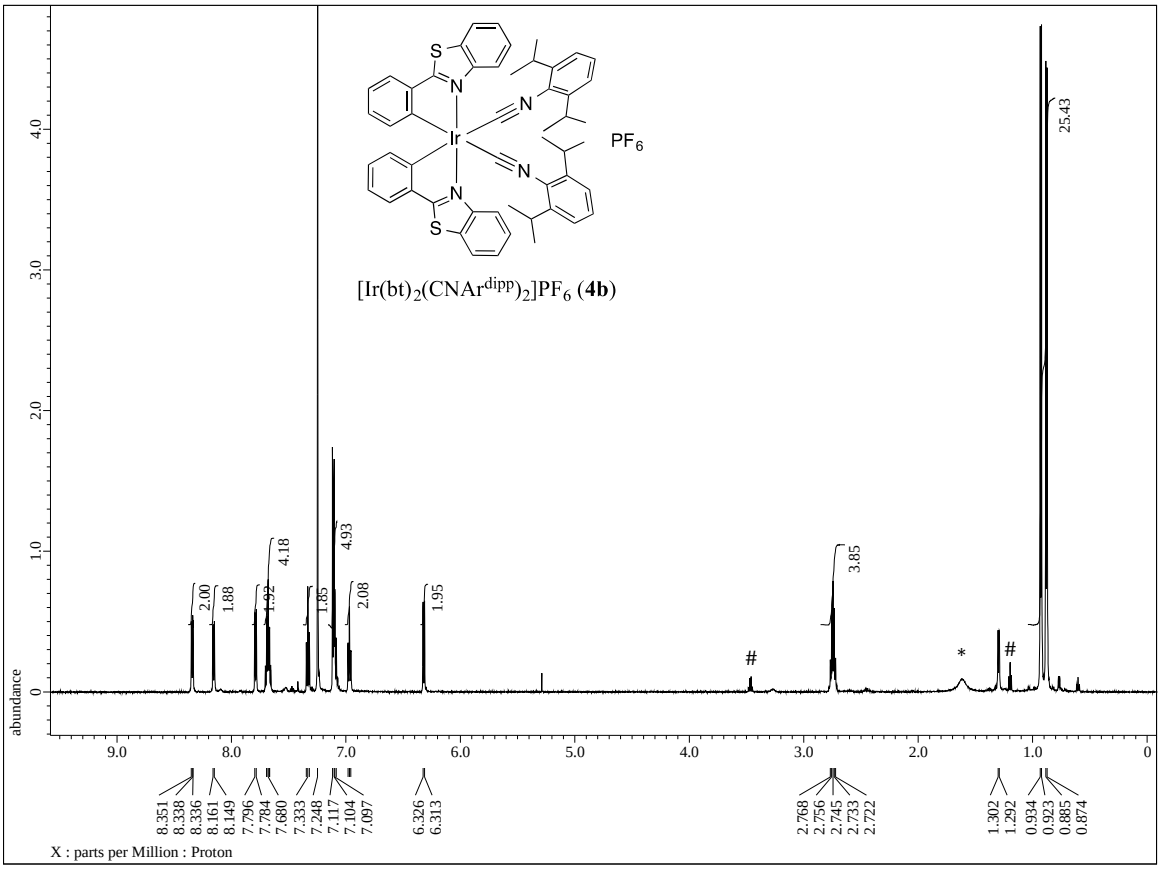

Figure S36. ^{1}H NMR spectrum of $[Ir(bt)_2(CNAr^{dipp})_2]PF_6$ (**4b**), recorded at 600 MHz in $CDCl_3$. Residual solvent peaks for diethyl ether (#) and water (*) are marked accordingly.

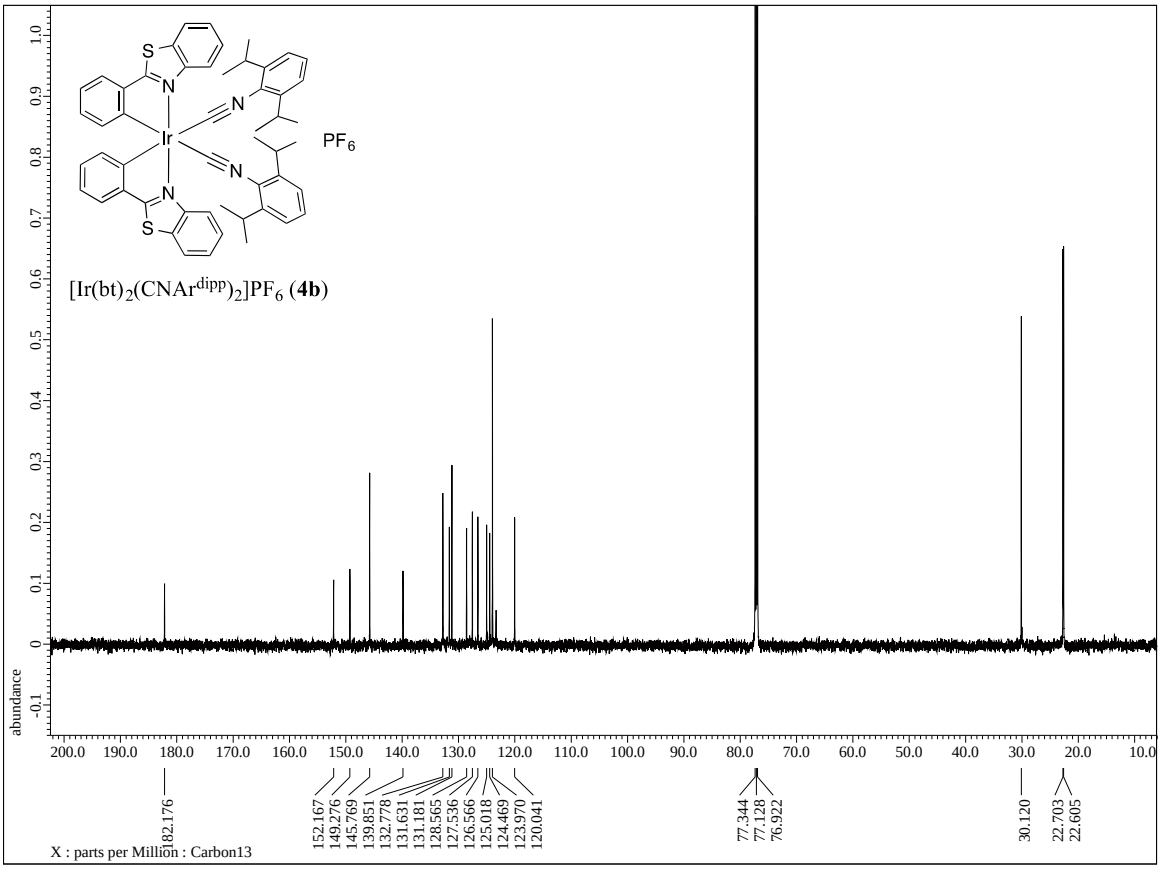

Figure S37. $^{13}C\{^{1}H\}$ NMR spectrum of $[Ir(bt)_2(CNAr^{dipp})_2]PF_6$ (**4b**), recorded at 151 MHz in $CDCl_3$.

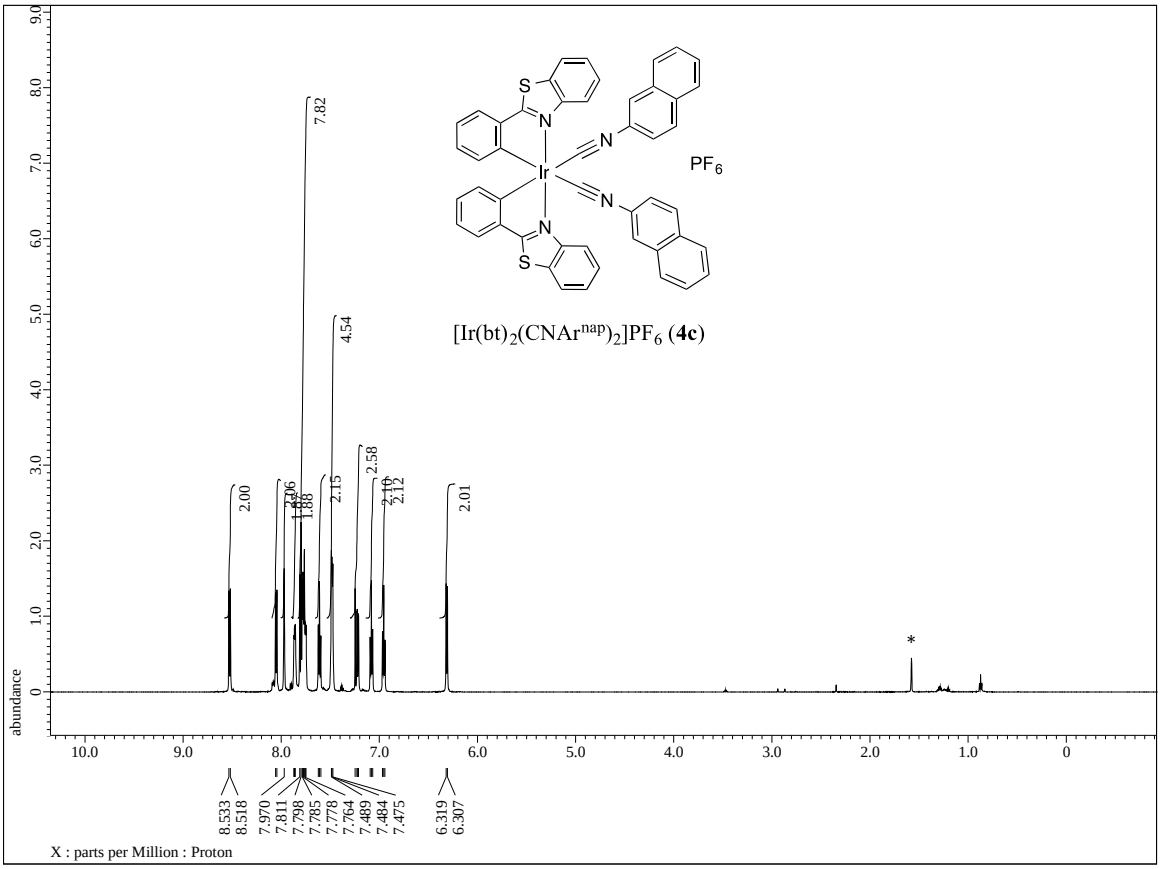

Figure S38. ^{1}H NMR spectrum of $[Ir(bt)_2(CNAr^{nap})_2]PF_6$ (**4c**), recorded at 600 MHz in $CDCl_3$. Residual solvent peak for water (*) is marked.

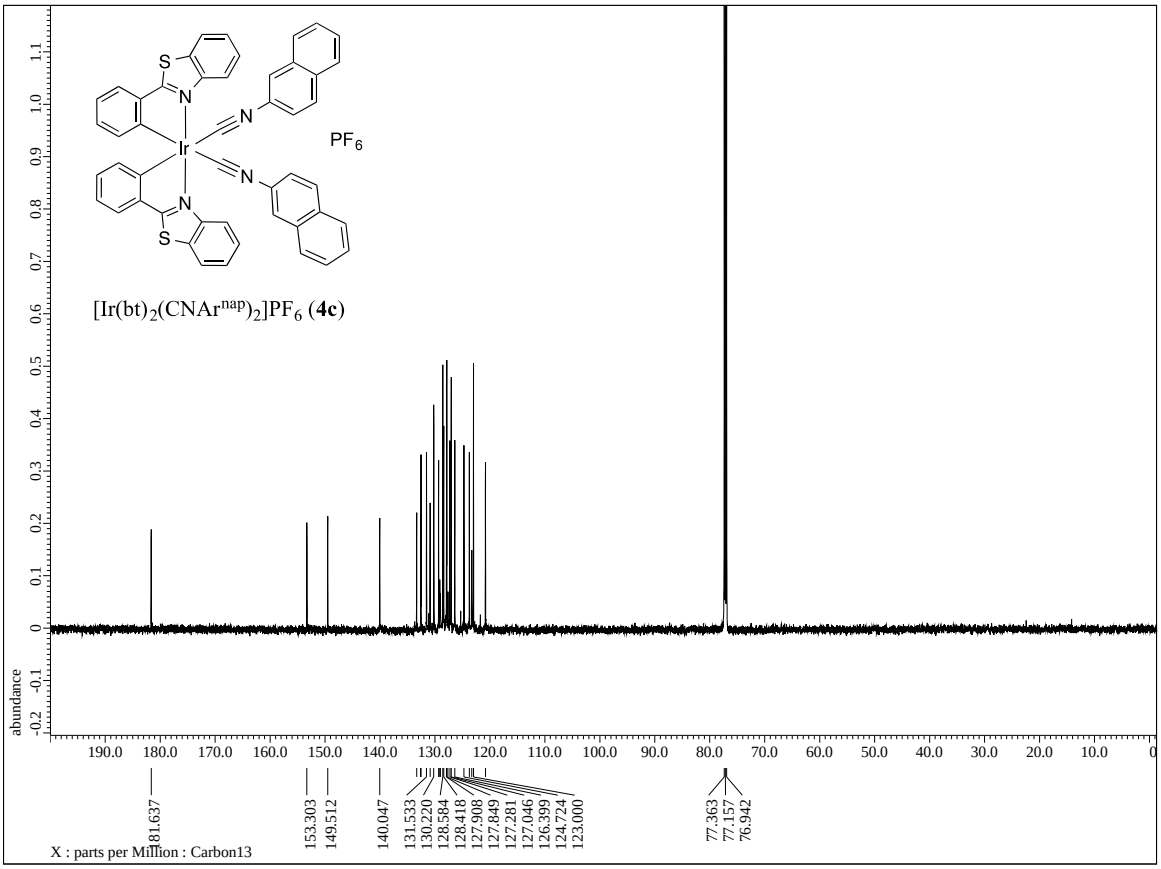

Figure S39. $^{13}C\{^{1}H\}$ NMR spectrum of $[Ir(bt)_2(CNAr^{nap})_2]PF_6$ (**4c**), recorded at 151 MHz in $CDCl_3$.